JOURNAL OF PETROLOGY | VOLUME 52 | NUMBER 1 | PAGES 113–146 | 2011 | doi:10.1093/petrology/egq075

Identification of Source Lithology in the Hawaiian and Canary Islands: Implications for Origins

CLAUDE HERZBERG*

DEPARTMENT OF EARTH AND PLANETARY SCIENCES, RUTGERS UNIVERSITY, 610 TAYLOR ROAD, PISCATAWAY, NJ 08854-8066, USA

RECEIVED APRIL 13, 2010; ACCEPTED OCTOBER 27, 2010
ADVANCE ACCESS PUBLICATION DECEMBER 2, 2010

Results are reported of an exploration of mantle source lithology for intraplate magmas using whole-rock and olivine phenocryst compositions. This analysis includes modern mid-ocean ridge basalts and Archean komatiites as low- and high-temperature reference frames. It is shown that the Ni, Ca, Mn, and Fe/Mn contents of olivine phenocrysts in modern mid-ocean ridge basalts and Archean komatiites are consistent with a normal peridotite source. In contrast, olivine phenocrysts in shield-building lavas on Hawaii are higher in Ni and Fe/Mn, and lower in Mn and Ca than those expected to crystallize from melts of a normal peridotite source, and point to the importance of pyroxenite as proposed by Sobolev and co-workers. Hawaiian shield stage lavas and their olivine phenocrysts are similar to those expected from partial melts of a 100% stage 2 pyroxenite source. Such a source might form from a variety of melt–rock, melt–melt, and rock–rock reactions. Primary pyroxenite-derived magmas have a range of SiO_2 contents that are positively correlated with $^{187}Os/^{188}Os$ and negatively correlated with $^{3}He/^{4}He$. These results are consistent with a Hawaiian plume containing recycled crust within a peridotite matrix. Variable amounts of free silica are inferred in Hawaiian pyroxenite sources, which contribute to the production of SiO_2-rich magmas. In contrast, peridotite and olivine pyroxenite melting are inferred to produce SiO_2-poor pre-shield magmas at Loihi. The interaction of SiO_2-rich and -poor magmas in the Hawaiian plume will trigger crystallization, not mixing. Mixing is permitted at low pressures in melt conduits and magma chambers, and work on olivine-hosted melt inclusions will be useful to evaluate its importance. In contrast to Hawaii, many ocean island basalts in localities such as the Canary Islands are deficient in SiO_2, and may have been generated by partial melting of olivine pyroxenites that formed by solid-state reaction between recycled crust + peridotite in the lower mantle. There is likely to be a wide range of whole-rock pyroxenite compositions in the mantle, as well as significant variability in Mn and Fe/Mn in both peridotite partial melts and their olivine phenocrysts. In general, there are not likely to be well-defined end-member peridotite and pyroxenite sources in the mantle. Nevertheless, taxonomical difficulties encountered in source lithology identification may yield rich rewards, such as a better understanding of the relationship between lithological diversity in the lower mantle and its petrological expression in intraplate magmatism.

KEY WORDS: *peridotite; pyroxenite; olivine; mantle*

INTRODUCTION

For years it was commonly assumed that mantle peridotite was the dominant source lithology that melted to produce basaltic magmas (Green & Ringwood, 1963; O'Hara, 1967). However, exposed pieces of the upper mantle show unambiguously the importance of 'pyroxenite' or 'eclogite' (Schulze, 1989; Hirschmann & Stolper, 1996; Kogiso *et al.*, 2004). Isotopic studies of intraplate oceanic islands have been used to infer the presence of recycled crust in their source region (Chase, 1981; Hofmann & White, 1982; Hauri, 1996; Chauvel *et al.*, 2008). However, it is not clear how the melting of recycled crust can be distinguished from the melting of metasomatized peridotite (Niu & O'Hara, 2003; Pilet *et al.*, 2008), especially if the metasomatizing agent originates from carbonated recycled crust (e.g. Dasgupta *et al.*, 2006, 2007; Jackson & Dasgupta, 2008; Walter *et al.*, 2008). Furthermore, if an oceanic island basalt is generated from a source that contained recycled crust that was completely mixed back into the mantle

*Corresponding author: Telephone: 732-445-3154. Fax: 732-445-3374. E-mail: herzberg@rci.rutgers.edu

peridotite during convective stirring (Jackson *et al.*, 2008; Gurenko *et al.*, 2009), then what criteria do we use to infer the involvement of recycled crust? Radiogenic heavy isotopes (Sr–Nd–Hf–Pb isotopes) combined with trace element evidence will tell us whether recycled crust is important, but cannot distinguish whether the crust is still present as a lithological unit in the source (pyroxenite), or whether only the geochemical signal of the recycled crust was imprinted onto the peridotite.

Identification of source lithology is important for a proper evaluation of estimates of mantle potential temperature in plumes (Herzberg & Asimow, 2008). When peridotite melts, the MgO content of the primary magma is positively correlated with both liquidus and mantle potential temperature (Langmuir *et al.*, 1992; Putirka, 2005; Herzberg *et al.*, 2007). As long as the water content of the source is low, high-MgO picrites and komatiites require hotter mantle to form than do basalts, and they have higher liquidus temperatures than basalts (Fig. 1a). The problem with this generally held view is that it holds only for peridotite sources. An equally hot pyroxenite source can produce melts with lower MgO (Fig. 1b; Herzberg, 2006).

The major issue is how to recognize recycled crust as a source lithology in the geochemical characteristics of a lava. Sobolev *et al.* (2005, 2007) suggested that the involvement of olivine-free pyroxenite, or eclogite, can be identified from the presence of olivine phenocrysts having high Ni, low Ca, and high Fe/Mn. However, there are a number of factors that can potentially compromise this interpretation. Kelemen *et al.* (1998) suggested that high-Ni olivines can be produced from peridotites that have reacted with dacitic melts. Li & Ripley (2010) suggested that temperature effects compromise inferences about source lithology. Wang & Gaetani (2008) suggested that high-Ni olivines could precipitate from eclogitic melts that equilibrate with mantle olivine. Olivines with high Fe/Mn might be an indicator of an iron-rich peridotite source (Humayun *et al.*, 2004) rather than pyroxenite (Sobolev *et al.*, 2007). Olivines with high Ca contents are thought to reflect a peridotite source (Herzberg, 2006; Sobolev *et al.*, 2007), but this will not be unique if some pyroxenite sources are rich in CaO. Additionally, if melts of pyroxenite and peridotite are able to leave the mantle separately, on what scale might they mix during transit to the crust?

This discussion is structured in several interrelated parts. The first is an analysis of peridotite partial melting and the Ni, Ca, Mn, and Fe/Mn contents of the olivine phenocrysts that can precipitate from the resultant melts. The second consists of an analysis of the possible solid-state transformations that might take place when oceanic crust is recycled in the Transition Zone and lower mantle. This provides a roadmap of the conceptual terrain, a means to sharpen our understanding of potential whole-rock source compositions that greatly influence partial melt and olivine phenocryst compositions. Finally, examples of pyroxenite and peridotite melting are explored with the aim of evaluating taxonomical methods of their identification (e.g. Sobolev *et al.*, 2007). Owing to the wealth of information on ocean islands, this paper is restricted to an analysis of Hawaii and the Canary Islands as representatives of high- and low-SiO_2 intraplate occurrences, respectively. The understanding of source lithology in the formation of Large Igneous Provinces is equally important, and this will be discussed in a subsequent study.

PERIDOTITE SOURCE PARTIAL MELTING

Computational method

Petrological solutions for batch and accumulated fractional melting of normal fertile peridotite were provided for SiO_2, Al_2O_3, FeO, MgO, and CaO (Herzberg & O'Hara, 2002; Herzberg, 2004, 2006). Normal mantle refers to pyrolite-like fertile peridotite (McDonough & Sun, 1995; Walter, 1998) having 0·25% NiO, 0·13% MnO and ~8% FeO. Primary magma solutions for MnO and NiO are given in this study.

The computational method was described by Herzberg & O'Hara (2002), and is analogous to calculating the liquid line of descent for any peridotite liquid composition. For each oxide, the compositions of olivine and orthopyroxene are calculated for the peridotite source as a total liquid, using the distribution coefficients of Herzberg & O'Hara (2002). The proportions of Ol and Opx are varied to reproduce the full range of possibilities for dunite and harzburgite residua, permitting the calculation of a bulk distribution coefficient. The peridotite liquid is allowed to crystallize in incremental steps, and the melt fraction F is mass balanced by the MgO content of the liquid, the residue, and the bulk peridotite composition. Liquid compositions for all oxides are calculated from solutions to the equations for batch and accumulated fractional melting for melt fractions in the ~0·23–1·0 range, for residues consisting of dunite and harzburgite. For melt fractions in the ~0–0·23 range, the relationship amongst melt fraction, FeO, and MgO are well described with equations (1)–(3) of Herzberg & Asimow (2008). Estimates of the SiO_2, Al_2O_3, and CaO contents (Herzberg, 2004, 2006) were provided for near-solidus melts by extrapolation of the high-quality experimental data of Walter (1998). Results at 3 GPa are in excellent agreement with the recent work of Davis *et al.* (2009) for all major elements. Unless otherwise stated, all primary magma compositions and the olivines that would crystallize from them are for the case of accumulated fractional melting, not batch melting.

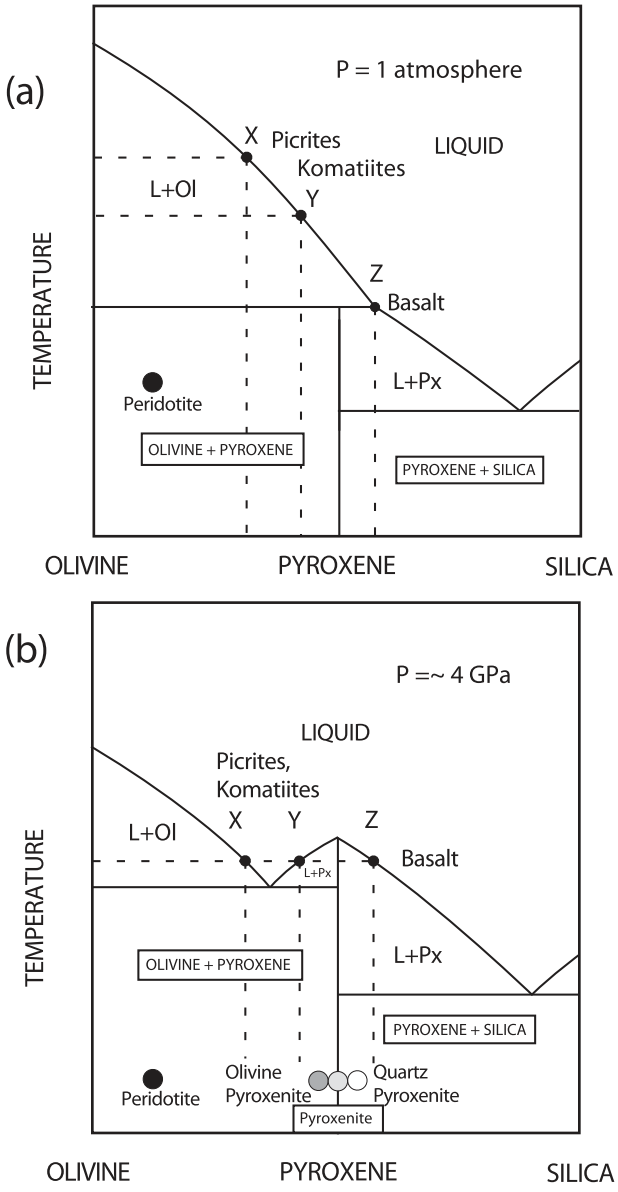

Fig. 1. Schematic pseudobinary Olivine–Silica diagram illustrating the important effects of increased pyroxene stability at high pressure, as discussed throughout the text. These are mainly: (1) partial melts of pyroxenite can require high temperatures, comparable with peridotite melting; (2) within the melting region, mixing X + Y is possible, but mixing Y + Z is not permitted; (3) commingling of Y + Z results in crystallization, not mixing. The effect of increased pressure on expanding the liquidus crystallization field of pyroxene at the expense of olivine is approximate, based on Kato & Kumazawa (1985) and Herzberg & Zhang (1998). It should be noted that the inference that mantle potential temperature T_P varies according to X > Y > Z is in error.

Ni contents of magmas and their olivine phenocrysts

The Ni contents of liquids for peridotite melting were calculated using a Jones–Beattie method for the olivine/liquid distribution coefficient: $D_{NiO}^{Ol/L} = 3{\cdot}346\ D_{MgO}O^{l/L} - 3{\cdot}665$ (Jones, 1984; Beattie *et al.*, 1991). The effect of temperature is captured in the compositional term $D_{MgO}^{Ol/L}$, and the constants are parameterized from experimental data (Beattie *et al.*, 1991). Other parameterizations exist (Hart & Davis, 1978; Kinzler *et al.* 1990), and there is an important level of agreement as summarized by Wang & Gaetani (2008) and Straub *et al.* (2008). In contrast, Li & Ripley (2010) reported a temperature-dependent Ni partitioning model that they suggested is better than the Jones–Beattie model; they concluded the pyroxenite interpretations of Sobolev *et al.* (2005, 2007) have been compromised by neglecting temperature effects. However, a closer look shows that the Jones–Beattie model actually provides a more accurate description of the experimental data than does the model of Li & Ripley (2010; see Electronic Appendix 1, available at http:www.petrology.oupjournals.org). More importantly, it will be shown that application of the Jones–Beattie model on modern mid-ocean ridge basalts (MORB) and Archean komatiites, extreme low- and high-temperature magmas respectively, reveals excellent agreement between predicted and observed olivine compositions.

Results for batch melting of fertile peridotite containing 1964 ppm Ni (0·25% NiO; McDonough & Sun, 1995) are given in Fig. 2 for L + Ol and L + Ol + Opx and near-solidus assemblages. Ni contents for near-solidus melts were calculated from the MgO contents of near-solidus melts (Herzberg & O'Hara, 2002) together with a solidus olivine composition having an mg-number of 89·5 (Walter, 1998; Herzberg & O'Hara, 2002) and 0·36% NiO (Ionov, 2007). It is notable that the Ni contents of near-solidus melts are nearly indistinguishable from those of melts for L + Ol and L + Ol + Opx assemblages, but this might be an artifact of using 0·36% NiO for solidus olivine. There is a significant range of Ni in olivine in mantle xenoliths (e.g. Ionov & Hofmann, 2007), and 0·36% NiO might be too high because of subsolidus partitioning into orthopyroxene (e.g. Herzberg, 1999).

There is a strong curvature to the MgO–Ni systematics at MgO > 30%, which reflects the change in the partitioning behavior of Ni from compatible to incompatible. Although partial melts of peridotite rarely contain MgO < 10% (Langmuir *et al.*, 1992; Herzberg *et al.*, 2007), the MgO–Ni curve is extended to 0% MgO to describe the systematics. For fertile peridotite similar in composition to KR-4003 (Walter, 1998; Herzberg & O'Hara, 2002) and 0·25% NiO, the Ni (ppm) content of primary accumulated fractional melts can be calculated from $Ni = 21{\cdot}6MgO - 0{\cdot}32MgO^2 + 0{\cdot}051MgO^3$ for MgO contents in the 0–25% range (Figs 2 and 3a). Ni contents of batch belts are nearly indistinguishable at MgO < 20%, but we will use results for accumulated fractional melting in all cases. Calculated Ni contents of accumulated fractional melts of depleted abyssal peridotite and fertile peridotites are indistinguishable at MgO contents in the

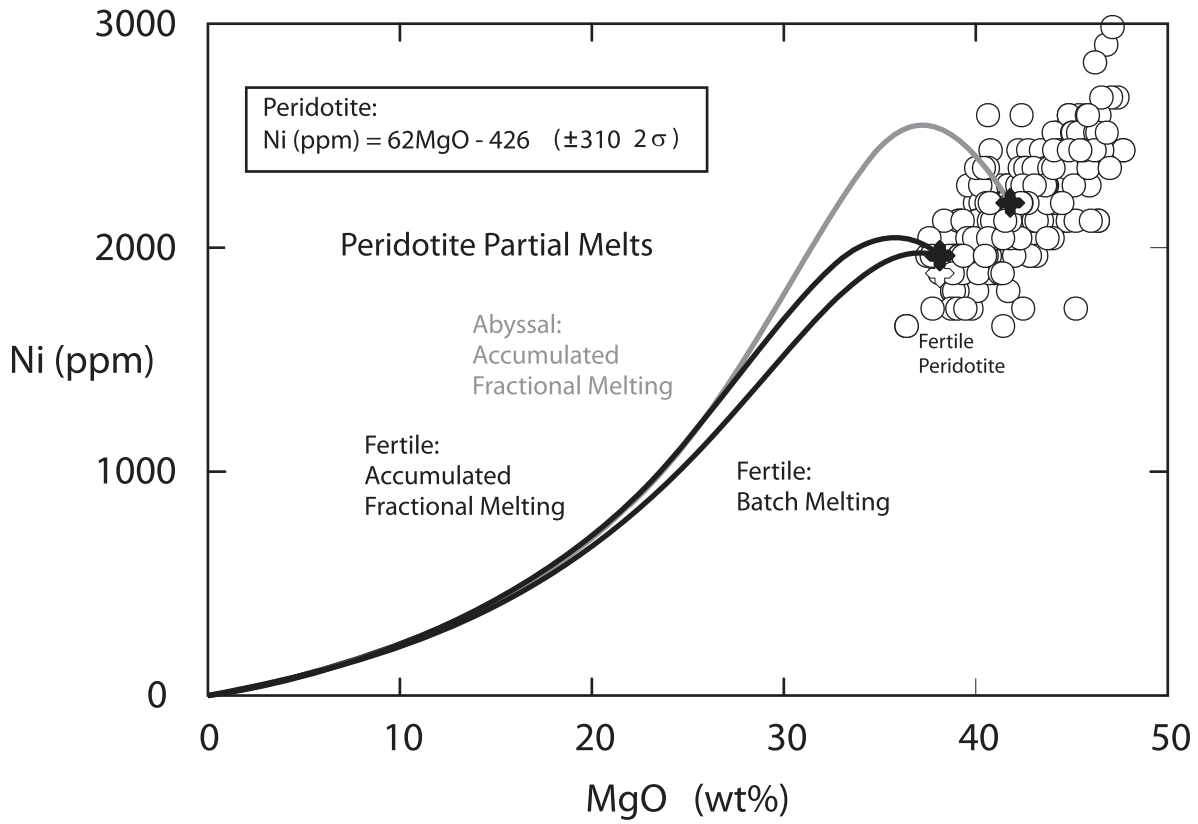

Fig. 2. MgO vs Ni contents calculated for partial melts of fertile and depleted peridotite having 1964 ppm Ni (0·25% NiO) and 2200 ppm Ni (0·28% NiO), respectively. The peridotite database (Herzberg, 1993) is described by the inset.

0–25% range (Fig. 2). However, in the peridotite database of Herzberg (1993), there is a significant range of Ni at any specific MgO content (Fig. 2; see also Ionov & Hofmann, 2007). This range in Ni propagates to calculated melt Ni variations shown in Fig. 3b.

The composition of olivine in equilibrium with both the primary magmas and their derivative liquids was calculated using olivine/liquid Ni distribution coefficients from Beattie *et al.* (1991), together with a 1 atm Fe/Mg exchange coefficient from Toplis (2005); the latter was chosen because it provides a good description of available experimental data over a wide pressure range (Herzberg *et al.*, 2007). Results are shown in Fig. 3b, and the effects of uncertainties in the Ni content of peridotite are given at the 2σ level. Olivines from primary magmas having 8–20% MgO contain 2700–3000 ppm Ni and have mg-numbers of 89–92 (Fig. 3b), in good agreement with the estimates of Straub *et al.* (2008). Olivines with mg-numbers >93 contain <3200 ppm Ni, reaching a low of ~1700 ppm for a total peridotite liquid. There is thus an inversion of the Ni content of olivine, with a maximum of 3200 ppm for olivines with mg-numbers of ~93 and, although not shown, a melt with this composition will form by about 50% accumulated fractional melting of fertile peridotite. In contrast, the model of Straub *et al.* (2008) shows no such maximum, but a progressive increase of Ni content with olivine mg-number. Furthermore, the results shown in Fig. 3b for primary magmas of fertile peridotite are nearly identical to those of depleted peridotite, except that olivines in the latter have even lower Ni and higher mg-numbers when the extent of melting approaches total. This result indicates that Fig. 3b is generally applicable to both fertile and depleted peridotite source compositions.

A comparison is now made of calculated and observed olivine compositions from the database of Sobolev *et al.* (2007). Some olivine phenocrysts from East Pacific Rise (EPR) MORB occurrences in the Garrett and Siqueiros fracture zones (Sobolev *et al.*, 2007) have nearly identical Ni contents to calculated olivines from primary magmas (Fig. 3b). Other EPR olivines have Ni contents that are much lower than those expected from fractional crystallization, and this might reflect the sequestration of Ni by a sulfide phase. Primitive olivine compositions from the Indian Ocean are similar to EPR olivines (Fig. 3b), but have lower mg-numbers and Ni contents. In general, the observed olivine phenocryst compositions are very similar to those expected of olivines that crystallize from primary MORB magmas with 10–13% MgO and their derivative

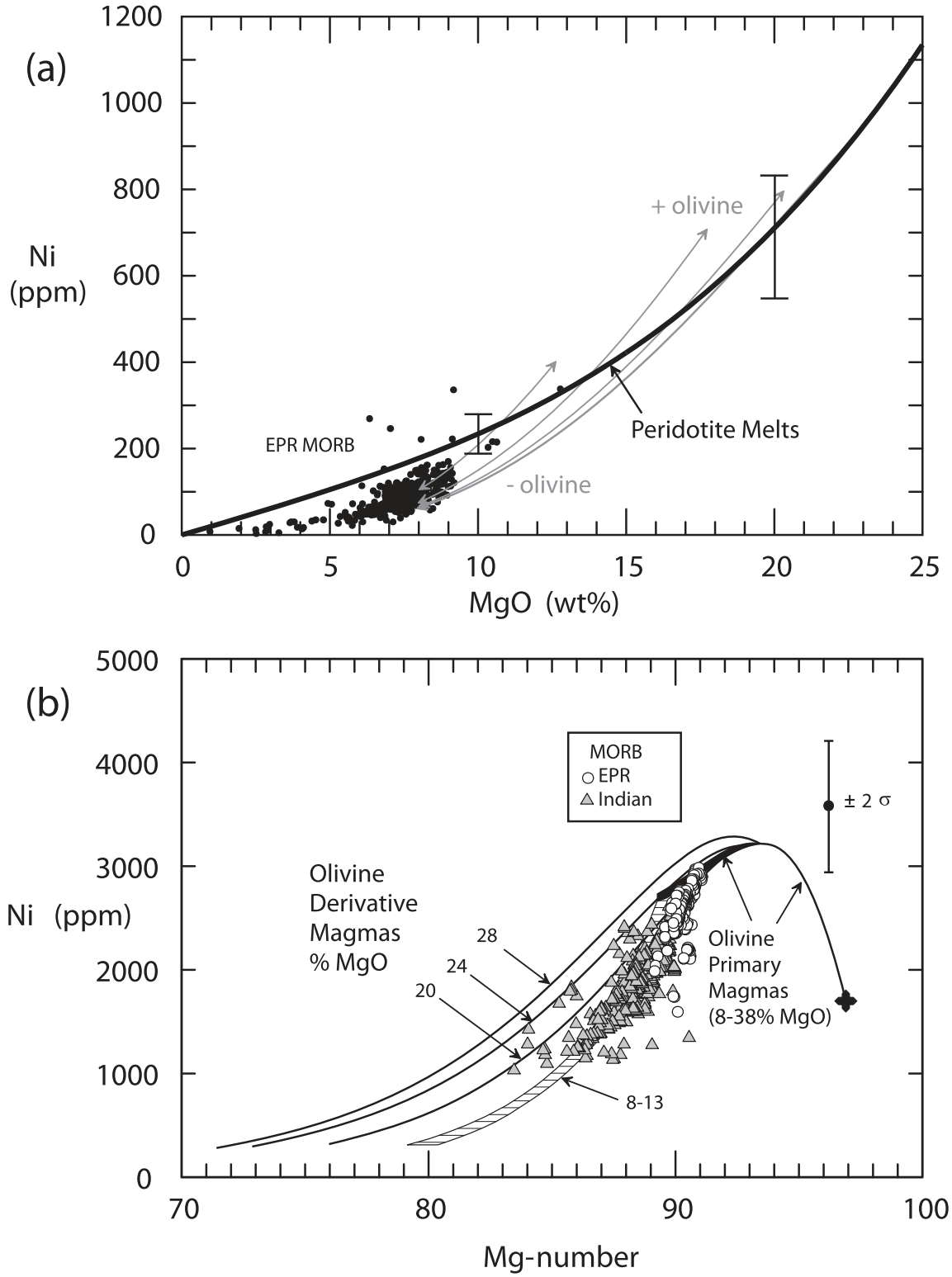

Fig. 3. (a) MgO and Ni contents for partial melts of fertile peridotite formed by accumulated fractional melting, from Fig. 2. Peridotite source contains 0·25% NiO (1964 ppm Ni). Uncertainties shown by the short lines with end-bars reflect the ±2σ variation in the Ni content of peridotite from Fig. 2. Grey arrows indicate olivine addition and subtraction. Black circles are EPR glasses from PETDB (http://www.petdb.org/). (b) Mg-number vs Ni content for calculated olivine (this work) and observed olivine (Sobolev *et al.*, 2007) phenocrysts. Calculated olivines are for both primary magmas of fertile peridotite with 1964 ppm Ni and derivative liquids produced by olivine fractionation. Black gooseneck curve is for calculated olivines of primary magmas of fertile peridotite with 1964 ppm Ni. Short line with end-bars reflects the ±2σ variation in the Ni content of the primary magmas from which the olivines crystallize. Horizontal hatched area indicates calculated olivines from olivine-fractionated derivative liquids with 8–13% MgO. Numbered lines are for calculated olivines from olivine-fractionated derivative liquids with 20–28% MgO.

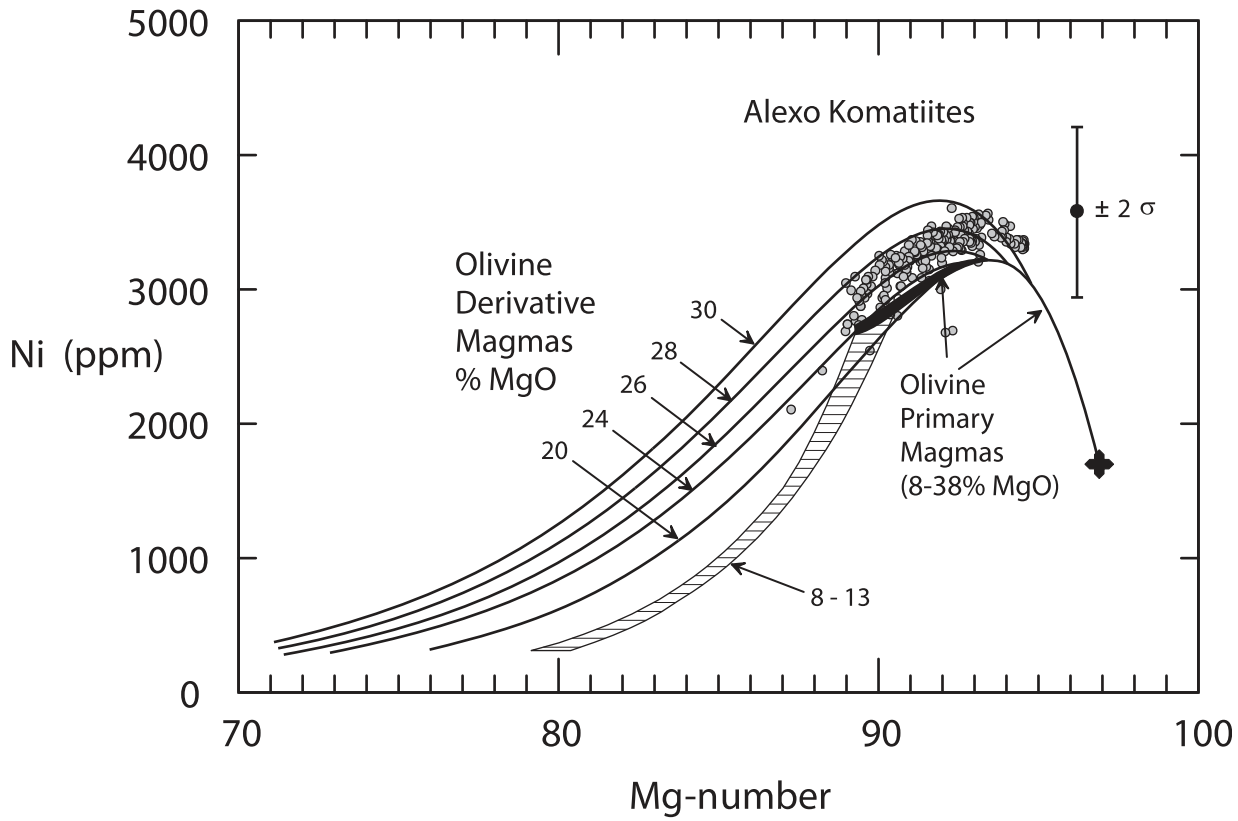

Fig. 4. Mg-number vs Ni content for calculated and observed olivine phenocrysts in the Alex komatiites (Sobolev *et al.*, 2007). Calculated olivines are for both primary magmas of fertile peridotite with 1964 ppm Ni and derivative liquids produced by olivine fractionation, as for Fig. 3. The excellent agreement between observed and calculated olivine phenocrysts that crystallized from liquids that formed from primary magmas with 28–30% MgO should be noted. This agreement is consistent with a peridotite source for the Alexo komatiites.

liquids. Some olivines from the Indian Ocean have Ni contents that might be interpreted as crystallizing from derivative liquids of primary magmas with 20–24% MgO (Fig. 3b). However, as shown below, it is the mg-number that is low, not Ni that is high, and this has probably resulted from Cpx fractionation in the crust and mantle. In this, and all cases discussed subsequently, the effects of Cpx fractionation are noted but not explicitly calculated. The major conclusion to be drawn from the Ni data is that MORB production is generally well described by peridotite melting. Some MORB olivines are higher in Ni (e.g. Romanche Fracture Zone), and for these Sobolev *et al.* (2007) inferred a minor role for pyroxenite melting.

Olivine phenocrysts from Alexo komatiites of Archean age have Ni contents that are somewhat higher than those expected in olivines crystallized from primary peridotite-source magmas (Fig. 4). However, they are very similar to olivines that crystallized from derivative liquids of primary magmas that had 26–30% MgO. This is consistent with previous estimates that Alexo komatiites crystallized from liquids with ~28% MgO (Puchtel *et al.*, 2004; Arndt *et al.*, 2008; Herzberg *et al.*, 2010). The sense of the systematics, concave toward the mg-number axis, is recognized for both calculated and observed olivines (Fig. 4). This remarkable level of agreement has several important implications. First, it indicates the Alexo komatiites melted from a peridotite source similar to the one we have modeled. The suggestion that some recycled crust was involved (Sobolev *et al.*, 2007) is not supported. Second, it provides evidence that the Jones–Beattie method of calculating Ni contents is successful in including temperature effects. The Alexo komatiites are thought to be some of the hottest magmas ever to have erupted on Earth (Arndt *et al.*, 2008; Herzberg *et al.*, 2010). They are compositionally similar to komatiites from the Belingwe greenstone belt (Puchtel *et al.*, 2009), for which melt inclusion studies point to a hot and dry origin (Berry *et al.*, 2008).

Ca contents of olivine phenocrysts

The Ca of olivine in equilibrium with both the primary magmas and their olivine-fractionated derivative liquids was calculated using olivine/liquid Ca distribution

coefficients from Herzberg & O'Hara (2002): $D^{Ol/L}_{CaO} = -0{\cdot}019 + 0{\cdot}007\ D^{Ol/L}_{MgO} + 0{\cdot}063/D^{Ol/L}_{MgO}$. As for Ni, this is a temperature-independent parameterization of experimental data. Additionally, olivine mg-number was calculated from the 1 atm Fe/Mg exchange coefficient from Toplis (2005). Results are shown in Fig. 5.

Olivine phenocryst compositions from East Pacific Rise MORB (Sobolev *et al.*, 2007) are very similar in composition to olivines calculated to crystallize from primary magmas (Fig. 5a), and there is good internal consistency with respect to Ni (Fig. 3b). Olivines from Indian Ocean MORB (Sobolev *et al.*, 2007) differ in being more similar to those expected to crystallize from derivative liquids, consistent with the Ni data. However, the effects of augite crystallization drive the Ca content down considerably (Fig. 5a) and contribute to the formation of liquids with lower mg-numbers. Augite crystallization can occur in both the crust and the mantle (Herzberg & Asimow, 2008).

Olivine phenocrysts from the Archean Alexo komatiites (Sobolev *et al.*, 2007) display roughly flat Ca trends, consistent with those expected of fractional crystallization of olivine from high-MgO liquids (Fig. 5b). However, the Alexo olivines have Ca contents that are 200–300 ppm higher than the calculated olivines, possibly pointing to compositional effects.

Mn and Fe/Mn of magmas and their olivine phenocrysts

Mn contents have been calculated for partial melts of KR-4003 peridotite (Walter, 1998) having 0·13% MnO, identical to the McDonough & Sun (1995) model pyrolite composition (Electronic Appendix 2; http:www.petrology.oupjournals.org). Results for accumulated fractional melting are shown in Fig. 6a. The composition of olivine in equilibrium with both these model primary magmas and their olivine-fractionated derivative liquids was calculated using Jones–Beattie olivine/liquid Mn distribution coefficients from Herzberg & O'Hara (2002), together with a 1 atm Fe/Mg exchange coefficient from Toplis (2005).

Olivine phenocrysts from the EPR have Mn and Fe/Mn that are similar to calculated olivines from primary melts of peridotite (Fig. 6b and c), similar to inferences drawn from Ni and Ca (Figs 3b and 5a). Mn and Fe/Mn for olivine from the Indian Ocean are also reasonably consistent with peridotite source melting. The advantage of exploiting Fe/Mn as a tracer is that both peridotite-source primary magmas and their derivative magmas yield olivines with Fe/Mn in the ~60–70 range, a result that is not likely to be significantly compromised by Cpx fractionation. However, some Indian MORB olivines have Fe/Mn < 60, and these might crystallize from more oxidized melts (Kelley & Cottrell, 2009).

For Archean komatiites, the inference of peridotite source melting based on the Ni and Ca contents in olivine (Figs 4 and 5b) is internally consistent with that based on Mn and Fe/Mn (Fig. 7). It is notable that olivine phenocrysts are similar to those expected from melts of a peridotite source with 0·13% MnO (Fig. 7b).

TRANSFORMATIONS OF OCEANIC CRUST DURING RECYCLING

Formation of pyroxenite by solid-state reaction

Most MORB contain <10% MgO, and high-quality partial melting experiments on such compositions at 3–5 GPa yield melt MgO contents in the 1–7% range (Pertermann & Hirschmann, 2003; Spandler *et al.*, 2008). In contrast, the primary magmas of oceanic islands have much higher MgO contents, typically 10–20% MgO (e.g. Hauri, 1996; Niu & O'Hara, 2003; Stolper *et al.*, 2004; Herzberg, 2006; Herzberg & Asimow, 2008). Therefore, the primary magmas of oceanic islands cannot form by direct partial melting of recycled basaltic oceanic crust. If it is true that recycled oceanic crust plays a role in intraplate volcanism, then it cannot be by direct partial melting. It has been suggested that partial melts of recycled basaltic oceanic crust react with peridotite to form a second-stage olivine-free pyroxenite, inferred to be the source of Hawaiian shield-stage volcanoes (Sobolev *et al.*, 2005), and that such pyroxenites can produce high-MgO primary magmas (Herzberg, 2006). An alternative possibility, examined here, is that second-stage pyroxenite might form by solid-state reaction between recycled crust and mantle peridotite.

Before we can proceed to understand how recycled oceanic crust can contribute to ocean island basalt (OIB) volcanism, it is necessary to have some idea of what happens to oceanic crust when it is subducted deep into the Transition Zone and lower mantle. One possibility is that it does not participate in OIB volcanism because it becomes permanently trapped in the lower mantle; this would be consistent with models that advocate recycled lithospheric peridotite as the source of OIB (e.g. Niu & O'Hara, 2003; Pilet *et al.*, 2008). Another possibility is that some of it might have been cycled through the lower mantle and returned to the surface in mantle plumes (e.g. Hofmann & White, 1982). To test these hypotheses from a petrological point of view, we need to understand the lithological changes that can potentially take place during the recycling of oceanic crust.

If the bulk basaltic oceanic crust remains isolated from the surrounding peridotite matrix, it will transform to a variety of garnet- and perovskite-bearing assemblages, all of which contain quartz, coesite, or stishovite (Irifune & Ringwood, 1993; Ono *et al.*, 2001; Pertermann & Hirschmann, 2003; Hirose *et al.*, 2005; Spandler *et al.*, 2008).

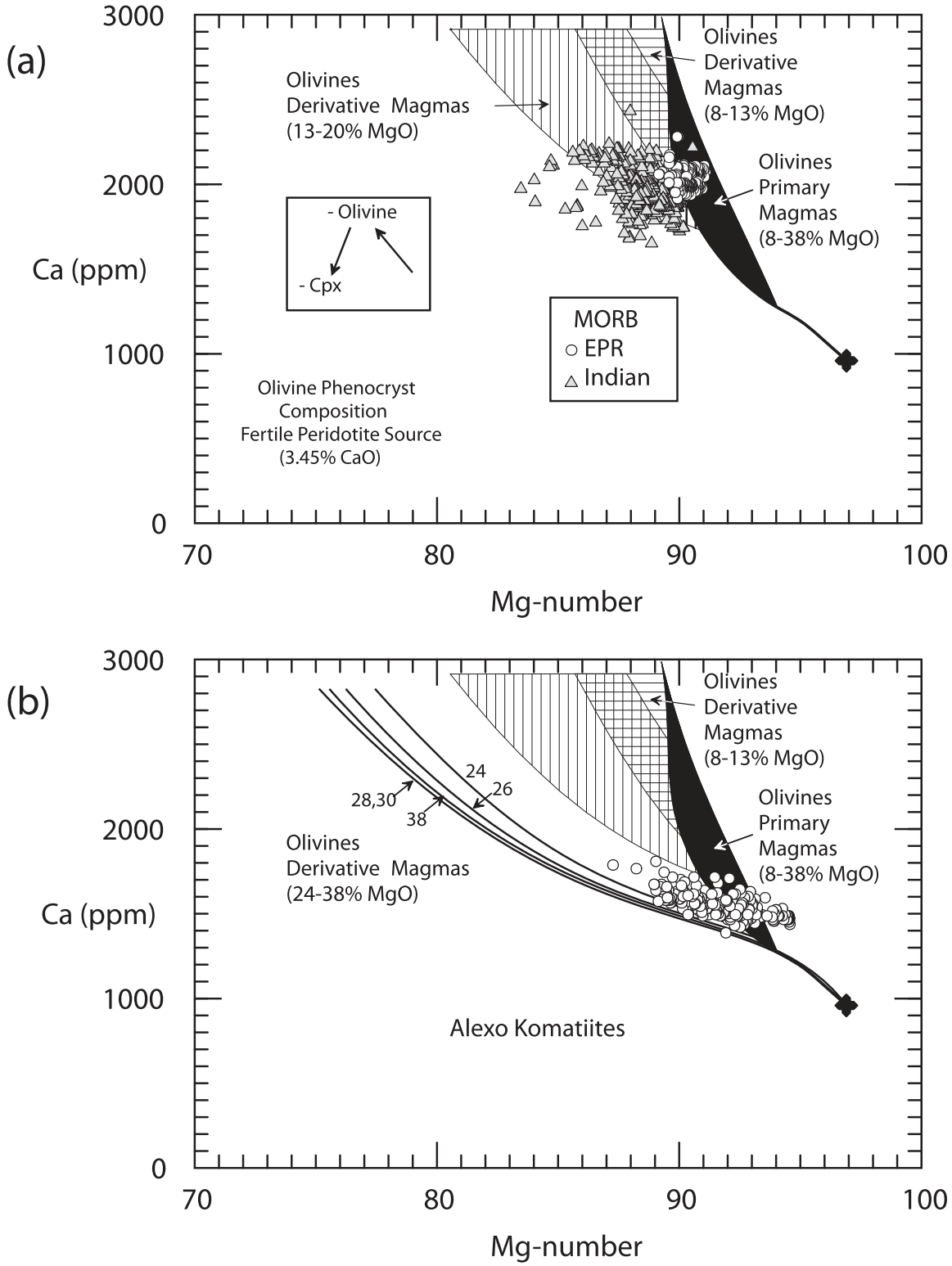

Fig. 5. Mg-number vs Ca content for calculated and observed olivine phenocrysts. Black area indicates calculated olivines of primary magmas derived from fertile peridotite with 3·45% CaO. Primary magmas are for accumulated fractional melting of fertile peridotite KR-4003 (Herzberg, 2006), and have 8–38% MgO. Horizontal hatched area indicates calculated olivines from olivine-fractionated derivative liquids with 8–13% MgO. Vertical hatched area indicates calculated olivines from olivine-fractionated derivative liquids with 13–20% MgO. (a) Olivines in MORB from the East Pacific Rise (Garrett and Siqueiros fracture zones) and Indian Ocean (Sobolev *et al.*, 2007); (b) olivines from Archean age Alexo komatiites (Sobolev *et al.*, 2007). Numbered lines are for calculated olivines from olivine-fractionated derivative liquids with 24–28% MgO (dunite residue).

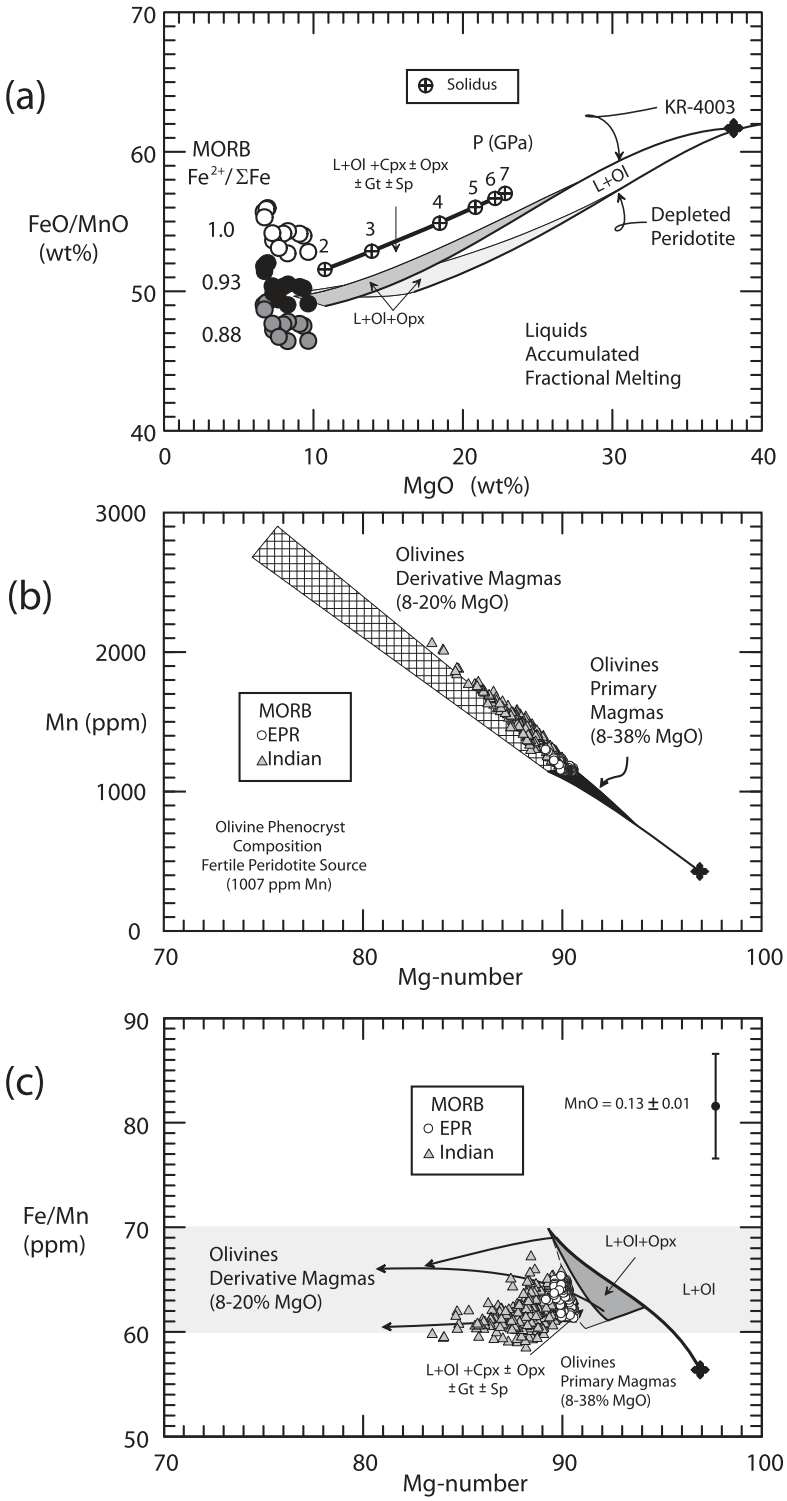

Fig. 6. (a) MgO vs FeO/MnO for melts of fertile peridotite based on experimental results from Walter (1998) on peridotite KR-4003, and a parameterization based on 0·13% MnO (1007 ppm Mn) and 8·02% FeO (Electronic Appendix 2). Results for the depleted abyssal peridotite composition are from Herzberg & O'Hara (2002) with FeO = 8·07% but with MnO = 0·13%. MORB glasses are from Qin & Humayun (2008) with $Fe^{2+}/\sum Fe = 0{\cdot}88–1{\cdot}00$ (by weight; Christie *et al.*, 1986; Bézos & Humler, 2005; Kelley & Cottrell, 2009). It should be noted that partial melts of peridotite have FeO/MnO in the ~50–60 range. Results shown for accumulated fractional melting are similar to those for batch melting. (b) Mg-number vs Mn content for calculated and observed olivine phenocrysts in MORB from the East Pacific Rise (Garrett and Siqueiros fracture zones) and the Indian Ocean (Sobolev *et al.*, 2007). Black area indicates olivines from primary magmas having 8–38% MgO for a peridotite source with 1007 ppm Mn. Cross-hatched area indicates olivines from olivine-fractionated derivative liquids having 8–20% MgO. (c) Mg-number vs Fe/Mn for MORB olivines. Left pointing arrows are examples of olivines in derivative liquids produced by olivine fractionation of primary magmas. Little change is expected for fractionation of Cpx. Grey area indicates typical olivine phenocrysts expected for a peridotite source with 0·13% MnO. L + Ol, L + Ol + Opx, and L + Ol + Cpx ± Opx ± Gt ± Sp designate the residuum mineralogy for accumulated fractional melts.

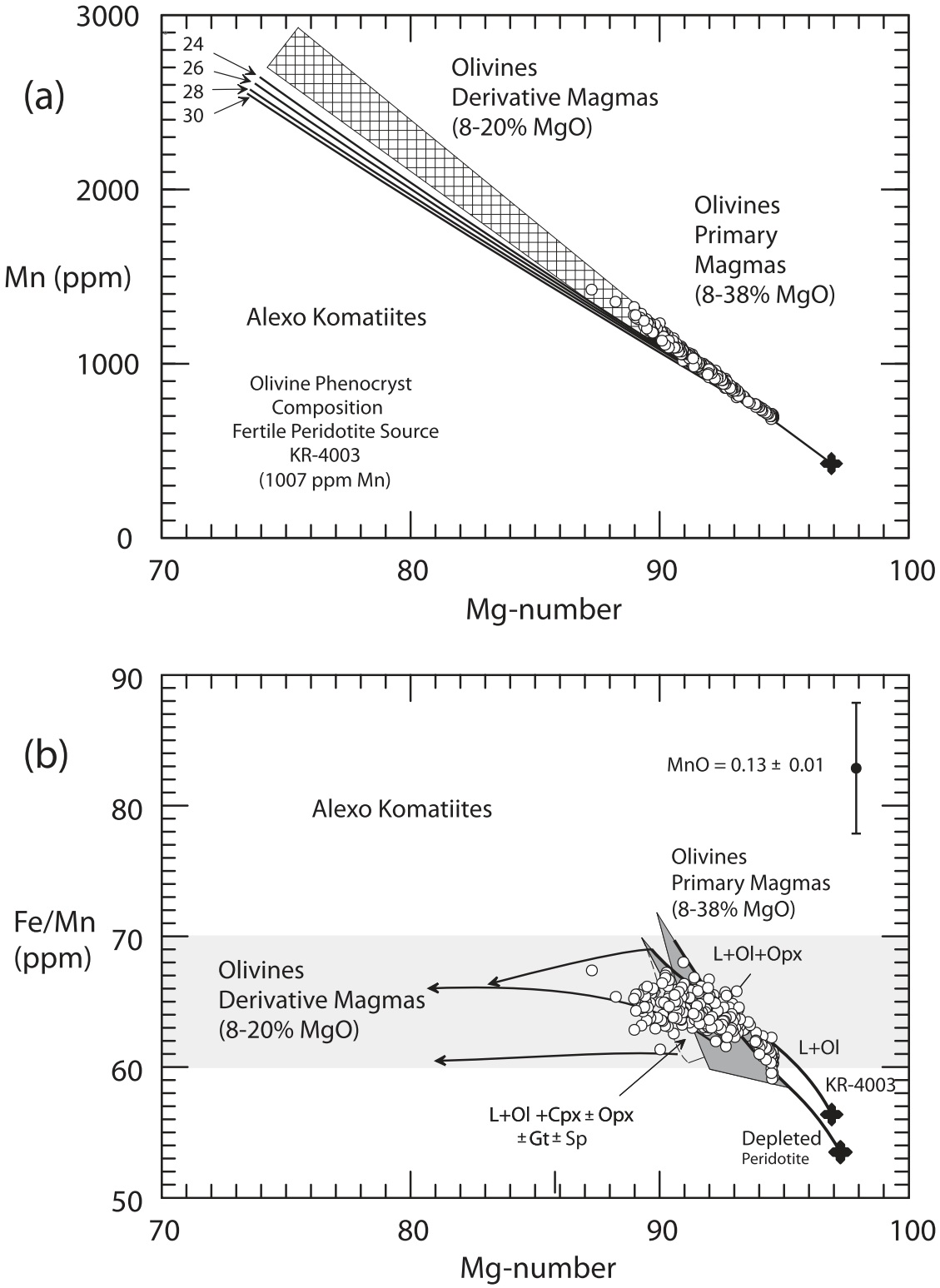

Fig. 7. (a) Mg-number vs Mn content for calculated and observed olivine phenocrysts in Alexo komatiites (Sobolev *et al.*, 2007). (b) Mg-number vs Fe/Mn for Alexo olivines. Excellent agreement between calculated and observed olivines supports the conclusion of a peridotite source for Alexo komatiites.

The transformation of basaltic crust produces quartz or coesite eclogite in the upper mantle,

$$\text{Plag} + \text{Cpx} + \text{Ol} = \text{Cpx} + \text{Gt} \pm \text{Opx} + \text{Quartz (coesite)} \quad (1)$$

and is here referred to as a stage 1 pyroxenite because SiO_2-rich differentiates of oceanic crust might have variable amounts of orthopyroxene. Garnet can become majoritic in the Transition Zone, but is referred to here simply as Gt. Reactions in a downgoing subducted slab in the lower mantle are expected to be similar to

$$\text{Cpx} + \text{Gt} \pm \text{Opx} + \text{Quartz (coesite)} = \text{MgPv} + \text{CaPv} + \text{CF} + \text{Stishovite}. \quad (2)$$

Within the lower mantle, the stage 1 pyroxenite will consist of Mg- and Ca-perovskite (MgPv and CaPv), stishovite, and CF (Ono *et al.*, 2001; Hirose *et al.*, 2005). CF is a silica-poor, sodium-rich aluminous phase with a calcium ferrite structure. Similar reaction products are expected at the core–mantle boundary where post-perovskite phases are stable (Hirose, 2006).

Oceanic crust also consists of cumulates of dunite, troctolite, and olivine gabbro; evidence for the participation of such materials in magma generation at Hawaii was given by Sobolev *et al.* (2000). Mass balance with respect to the EPR primary magma composition (Herzberg *et al.*, 2007) yields cumulates that are MgO-rich, and most plot between the garnet–pyroxene plane and the perovskite–CF plane (Fig. 8). These will consist of olivine pyroxenite lithologies (Ol + Cpx + Gt) in the upper mantle and Transition Zone, and stishovite perovskite lithologies in the lower mantle (Fig. 8).

Convective mixing and stirring will fold, stretch, and thin this crust (Allègre & Turcotte, 1986; van Keken & Zhong, 1999; Farnetani *et al.*, 2002; Graham *et al.*, 2006). When this happens, solid-state reactions will occur because the silica-bearing recycled crust lithology is not stable in an olivine-rich peridotite host. Reactions of the general type olivine + free silica = orthopyroxene will occur between the recycled crust and host peridotite producing a stage 2 pyroxenite. In the lower mantle, the reaction will be ferropericlase (Mg,Fe)O + stishovite SiO_2 = magnesium perovskite.

Stage 2 pyroxenite reactions will occur without fail at the contacts between silica-rich recycled crust and the host peridotite (Fig. 8) through reactions of the type

$$\text{Crust} + \text{Peridotite} = \text{Cpx} + \text{Gt} \pm \text{Opx} \quad (3)$$

$$\text{Crust} + \text{Peridotite} = \text{MgPv} + \text{CaPv} + \text{CF}. \quad (4)$$

The open and closed circles in Fig. 8 represent stage 2 pyroxenites within the garnet–pyroxene plane and the perovskite–CF planes, respectively.

An important consideration is that silica-bearing lithologies will probably remain if they are deeply buried within a thick crustal package and isolated from the surrounding peridotite. Solid-state reactions will not go to completion, and the formation of stage 2 pyroxenite with free silica can be represented by

$$\text{Crust} + \text{Peridotite} = \text{Cpx} + \text{Gt} \pm \text{Opx} + \text{Quartz (coesite)} \quad (5)$$

$$\text{Crust} + \text{Peridotite} = \text{MgPv} + \text{CaPv} + \text{CF} + \text{Stishovite}. \quad (6)$$

Whether free silica remains in the pyroxenite will probably be influenced by the size of the bodies, which are expected to be reduced on stretching and thinning during convective stirring in the mantle. As discussed below, this will have important consequences for the compositions of any magma produced by the melting of stage 2 pyroxenite. In particular, it will determine whether an oceanic island can potentially form from primary magmas that are silica-rich or silica-poor (e.g. Kogiso *et al.*, 2004; Herzberg, 2006; Jackson & Dasgupta, 2008).

Most high-MgO crustal cumulates will become olivine pyroxenites in the upper mantle and Transition Zone (Ol + Cpx + Gt). However, they may react with peridotite in the lower mantle according to equation (4).

Should subducted oceanic crust be incorporated into a rising mantle plume and returned to the upper mantle, all stage 2 pyroxenites consisting of MgPv + CaPv + CF will transform to olivine pyroxenite via the reaction

$$\text{MgPv} + \text{CaPv} + \text{CF} = \text{Ol} + \text{Cpx} + \text{Gt}. \quad (7)$$

These pyroxenites plot to the SiO_2-poor side of the pyroxene–garnet plane and are referred to as SiO_2-poor and olivine pyroxenites here. In general, olivine pyroxenite lithologies are expected to be abundant in recycled crust that has been stirred, stretched and thinned, and they have the potential to yield low-SiO_2 alkalic oceanic island basalts. In contrast, any pyroxenite that has free SiO_2 in the upper mantle and Transition Zone will plot to the SiO_2-rich side of the pyroxene–garnet plane, and has the potential to melt to produce SiO_2-rich tholeiitic basalts. Hawaii and the Canary Islands provide good examples of SiO_2-rich and -poor pyroxenite-source lavas, respectively, as discussed below.

We can imagine a complete range of reaction and mixing possibilities involving free silica (Fig. 8), and discuss specific examples below. In the case where all free silica reacts out, the mantle will consist of peridotite and layers of either silica-free pyroxenite (Cpx + Gt ± Opx) or olivine pyroxenite (Cpx + Gt + Ol). This is the marble cake model of Allègre & Turcotte (1986), except that it differs in having been substantially reconstituted and is free of a silica-rich phase. There may be substantial

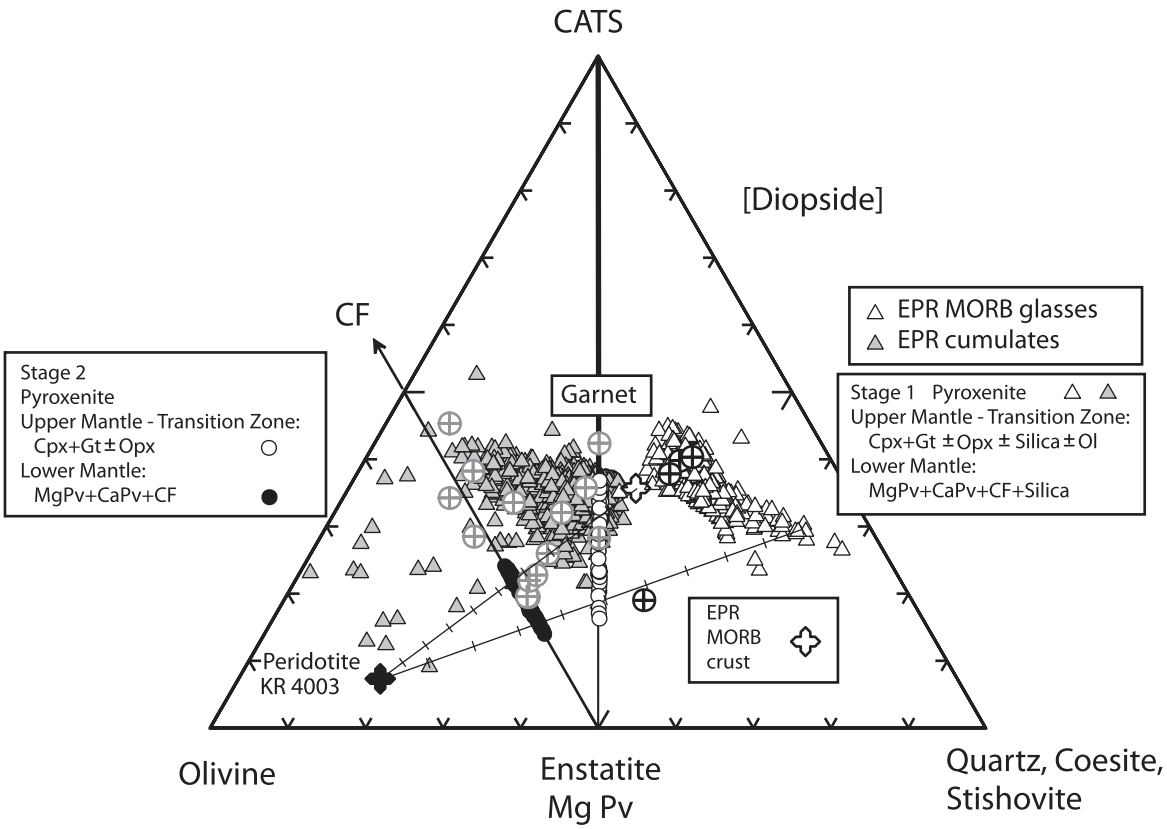

Fig. 8. Mole per cent projection of various glass and whole-rock compositions from or towards Diopside into the plane Olivine–Quartz–Calcium Tschermak's (CATS). White triangles, projected 3467 MORB glass compositions from the East Pacific Rise (http://www.petdb.org/); grey triangles, projected troctolite and gabbro cumulates for 3467 EPR MORB glasses calculated from mass balance and assuming a primary magma with 11·8% MgO (Herzberg *et al.*, 2007); crosses in circles, pyroxenite compositions for which high-pressure experimental data are available (see text) (black, silica-rich compositions; grey, silica-poor compositions). Open circles, stage 2 pyroxenites formed in the upper mantle and Transition Zone by the solid-state reaction of MORB with fertile peridotite KR-4003; these are coincident with the Diopside–Enstatite–CATS plane (pyroxene–garnet plane). The pyroxene–garnet plane is used for taxonomical purposes to identify high- and low-SiO_2 pyroxenites on the SiO_2-rich and -poor sides, respectively. Filled circles, stage 2 pyroxenites formed in the lower mantle by the solid-state reaction of MORB with fertile peridotite KR-4003; these are coincident with the Ca and Mg perovskite–CF plane, where CF is an aluminous phase with the calcium ferrite structure. Also possible but not shown for clarity are stage 2 pyroxenites that may form on the Ca and Mg perovskite–CF plane by the reaction of EPR MORB cumulates with peridotite. The mole per cent projection is derived from the code given by O'Hara (1968): Olivine (OL) $= 0{\cdot}5(Al_2O_3 + Cr_2O_3 + FeO + MnO + NiO + MgO) - 0{\cdot}5(CaO + Na_2O + K_2O) + 1{\cdot}75P_2O_5$. CATS $= TiO_2 + Al_2O_3 + Cr_2O_3 + Na_2O + K_2O$. Quartz (QZ) $= SiO_2 + TiO_2 + 0{\cdot}5(Al_2O_3 + Cr_2O_3) - 0{\cdot}5(FeO + MnO + MgO + NiO) - 1{\cdot}5CaO - 4{\cdot}5(Na_2O + K_2O) + 5{\cdot}25P_2O_5$.

mixing between peridotite and pyroxenite layers, and olivine pyroxenites might grade into refertilized peridotite. In the extreme, complete mixing might destroy all remnants of the original recycled crust.

Compositions of model whole-rock pyroxenites and their partial melts

A calculation has been made of stage 2 pyroxenite whole-rock compositions contained in the planes pyroxene–garnet and perovksite–CF by adding silica-rich MORB crust and glasses to peridotite according to reactions (3) and (4). Results are presented in Figs 9 and 10a. These are compared with experimentally determined partial melt compositions of a wide variety of pyroxenite compositions at pressures in the 2–5 GPa range (Longhi, 2002; Salters *et al.*, 2002; Hirschmann *et al.*, 2003; Kogiso *et al.*, 2003; Pertermann & Hirschmann, 2003; Keshav *et al.*, 2004; Kogiso & Hirschmann, 2006; Sobolev *et al.*, 2007; Yaxley & Sobolev, 2007; Spandler *et al.*, 2008). The important observation is that there is a wide range of potential whole-rock pyroxenite compositions, and this will propagate to both their partial melts and crystallizing olivines.

MgO and FeO contents

Stage 2 pyroxenite compositions on the Di–En–CATS plane have lower MgO contents than those on the CaPv–MgPv–CF plane, although both have FeO contents >8%

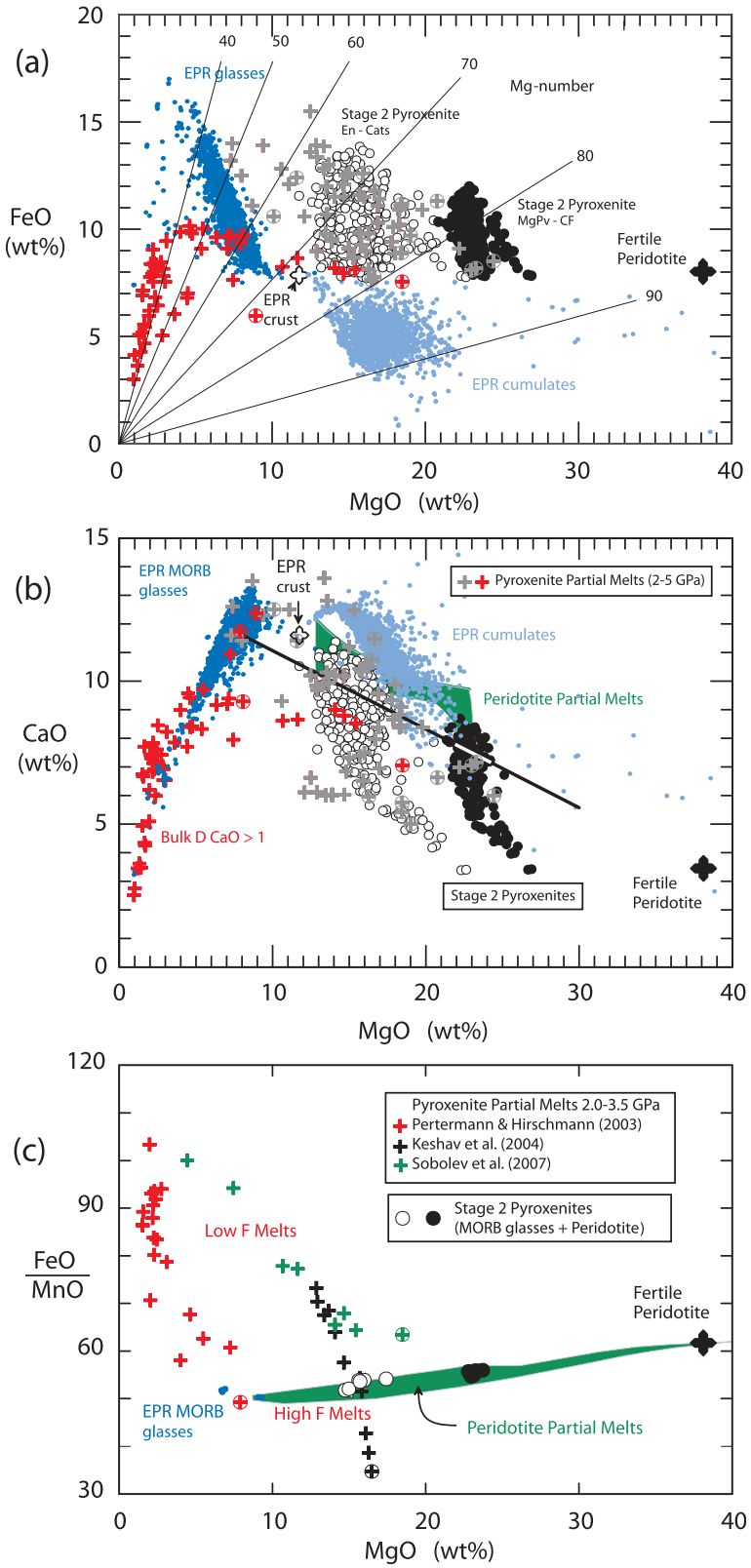

Fig. 9. Compositional diversity of potential stage 2 pyroxenites formed by solid-state reaction. (a) FeO and MgO contents and mg-numbers. Red and grey crosses are experimental melt compositions of SiO_2-rich and -poor pyroxenites, respectively. Crosses in circles are starting material compositions of these experiments. Open and closed circles are defined in Fig. 8. (b) Peridotite- and pyroxenite-source primary magmas were proposed to plot on the high- and low-CaO sides of the line (Herzberg & Asimow, 2008), but this is likely to hold only for certain high-SiO_2 pyroxenite melts (see text). (c) Selected experimental data showing the effect of melt fraction on FeO/MnO of pyroxenite partial melts.

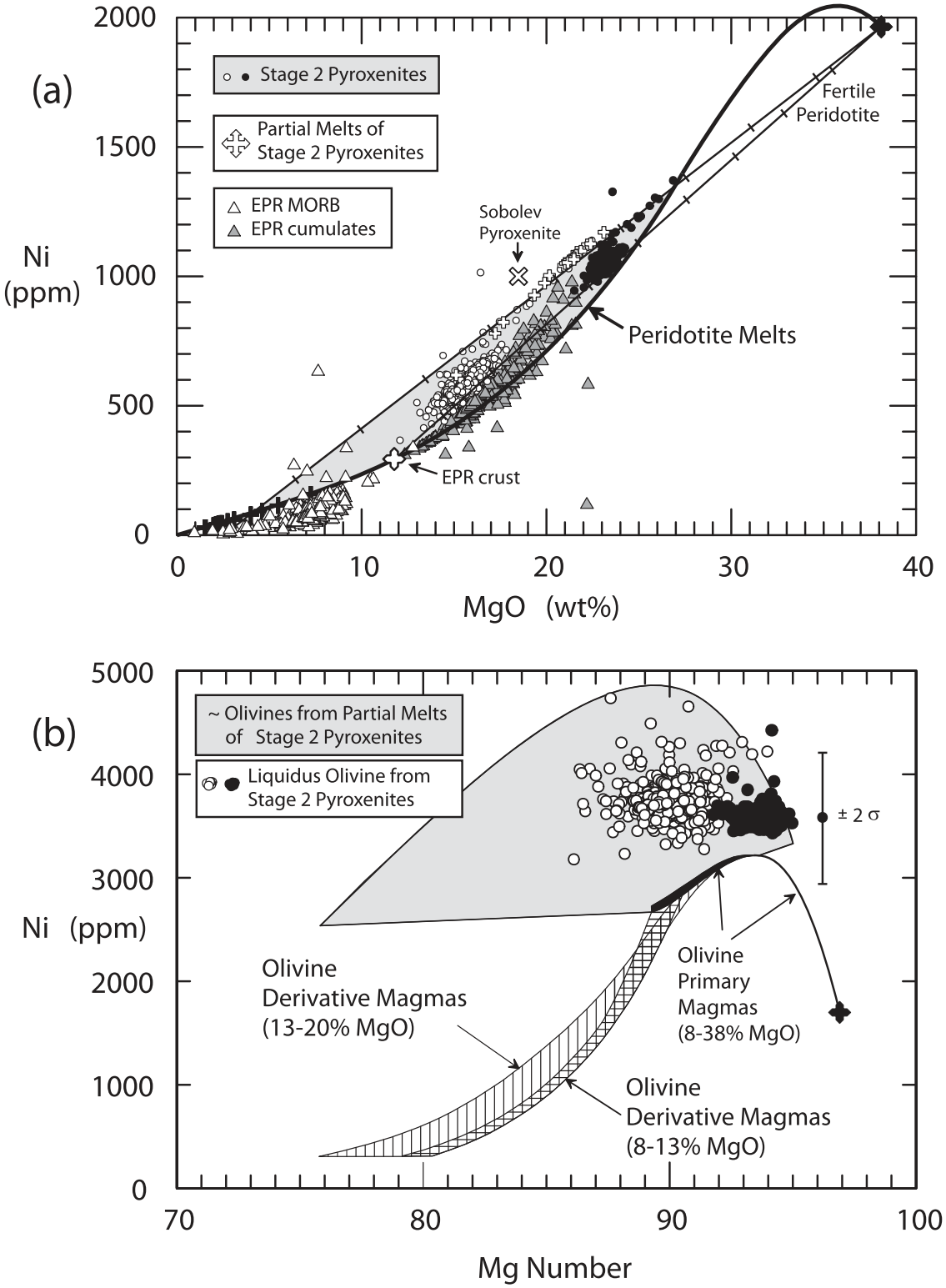

Fig. 10. Ni contents of melts and olivine phenocrysts for peridotite and pyroxenite sources. (a) Open and closed circles are the same as for Fig. 8, and refer to whole-rock Ni contents of stage 2 pyroxenites formed on the pyroxene–garnet and Ca and Mg perovskite–CF planes, respectively. Ni contents for peridotite partial melts are from Figs 2 and 3a, for accumulated fractional melting of a peridotite with 0·25% NiO. The two mixing lines for peridotite–MORB shown at 10% increments (tick marks) are the same as those given in Fig. 8. Open 'X' is whole-rock pyroxenite composition from Sobolev *et al.* (2007). Black crosses (+), partial melts of MORB at 3 GPa (Pertermann & Hirschmann, 2003) calculated to be in equilibrium with olivine having 2828 ppm Ni. Open crosses, stage 2 pyroxenites on the pyroxene–garnet plane formed by reacting partial melts of MORB with peridotite. Grey shading delineates the wide range of possible whole-rock Ni contents for stage 2 pyroxenite; partial melts can have an even wider range of compositions (see text). (b) Ni contents of olivines for peridotite melts and their olivine-fractionated derivative liquids from Figs 3b and 4. Grey shading delineates liquidus olivine compositions that would crystallize from total melts of pyroxenite compositions in (a).

and mg-numbers in the 70–85 range (Fig. 9a; note that En and MgPv are compositionally equivalent to enstatite). It can be shown that these mg-numbers are approximately the same as those expected of olivines that would crystallize from initial melts of these pyroxenites (70–85). Should the pyroxenites become totally melted, the olivines that would crystallize would have mg-numbers in the 87–95 range. Olivine mg-numbers of 70–95 are therefore expected to crystallize from pyroxenite melts formed under conditions that range from initial to total melting. It is clear that a specific olivine mg-number cannot be used to constrain a primary magma of a pyroxenite source. This will be a source of significant error in any method that calculates parental magma composition by adding olivine until the melt is in equilibrium with olivine having an mg-number of 90, for example. The problem is similar to that of magmas that are produced by partial melting of sources that consist of cumulates (Fig. 10a) or any pyroxenite that is derived from such cumulates.

The FeO contents for stage 2 pyroxenite can range from ~3 to 13%. This is likely to have major geodynamic consequences for compositional buoyancy. Some of the more FeO-rich examples might be too dense to be sampled by mantle plumes, and may permanently reside in the lower mantle. In contrast, FeO-poor pyroxenites are expected to be buoyant. The implication is that a compositionally heterogeneous lower mantle might be selectively sampled by mantle plumes.

CaO contents

The importance of pyroxenite melting in the generation of Hawaiian shield-building lavas has been inferred on the basis of high Ni contents in olivine (Sobolev *et al.*, 2005, 2007) and low whole-rock CaO contents (Herzberg, 2006). Most primitive shield-building lavas from Hawaii have CaO contents that are lower than model CaO contents of peridotite-source melts (Herzberg, 2006); the discriminent line shown in Fig. 9b was proposed as a way to discriminate peridotite-source lavas above from pyroxenite-source lavas below (Herzberg & Asimow, 2008). The inference of pyroxenite melting for Hawaii based on low-CaO and high-Ni olivines is supported here, as discussed in more detail below. However, it is now clear that this conclusion cannot be generalized to all cases of pyroxenite melting. Although it is true that many stage 2 pyroxenite sources have low CaO contents, other pyroxenites can be high in CaO and plot above the discrimination line in Fig. 9b. Clearly, a high-degree melt of a high-CaO pyroxenite can have CaO contents that are similar to those of peridotite-source melts.

More experimental data are needed to parameterize the effects of pyroxenite composition and melt fraction on the CaO content of partial melts. However, a few general points can be made. Pyroxenite source compositions that plot to the SiO_2-rich side of the pyroxene–garnet plane in Fig. 8 have bulk distribution coefficients for CaO, *D* CaO Solid/Liquid, that are generally >1 (Fig. 9b). Partial melts of these high-silica pyroxenites display MgO–CaO systematics that are similar to those of MORB (Fig. 9b). That is, low-degree melts of SiO_2-rich pyroxenite are generally low in CaO owing to the dominant effect of residual clinopyroxene. At the other extreme is peridotite melting, where low-degree melts are always enriched in CaO (Fig. 9b) and *D* CaO is <1. Clearly, the amount of clinopyroxene in the residue has a large effect on bulk *D*, and between these extremes are stage 2 pyroxenites.

Some pyroxenites and their partial melts have high CaO contents (Hirschmann *et al.*, 2003; Kogiso *et al.*, 2003; Keshav *et al.*, 2004; Kogiso & Hirschmann, 2006), similar to those of peridotite-source lavas (Fig. 9b). However, the pyroxenites in these experimental studies are similar in composition to rocks that have been interpreted to be cumulates that precipitated deep within the mantle (Frey, 1980; Irving, 1980; Sen, 1988; Keshav *et al.*, 2007). Although they are useful for parameterization purposes, the melting of these high-CaO pyroxenites is not likely to be relevant to the general understanding of the role played by recycled crust in oceanic island magmatism.

FeO/MnO

Peridotite and its partial melts have FeO/MnO in the 50–60 range (Figs 6a and 9c). Stage 2 pyroxenites have similar FeO/MnO, calculated from high-precision inductively coupled plasma–mass spectrometry analyses for Mn from MORB EPR glasses (Qin & Humayun, 2008; $Fe^{2+}/\sum Fe = 0{\cdot}93$). In contrast, melting experiments on pyroxenite lithologies that contain $Cpx + Gt \pm Opx \pm Qz$ display a wide range of FeO/MnO ratios in the melt, many of which are higher than the range for peridotite (Liu *et al.*, 2008). Of the existing dataset for pyroxenite melting, those of Pertermann & Hirschmann (2003), Keshav *et al.* (2004) and Sobolev *et al.* (2007) are most helpful in revealing how FeO/MnO varies with melt fraction (Fig. 9c). FeO/MnO can be high at low melt fractions, typically exceeding 80. FeO/MnO is high because MnO is low, not because FeO is high. Partial melts of pyroxenite are low in MnO when the modal amount of garnet in the residuum is high, and this depends on the whole-rock composition and melt fraction. As *D* Mn Gt/L ranges from seven at low *F* to about two in the experiments of Pertermann & Hirschmann (2003), Mn is retained in residual garnet rather than expelled to the melt. A similar conclusion has been drawn by Balta *et al.* (2010).

It has been suggested that olivine phenocrysts with elevated Fe/Mn indicate a pyroxenite-source lithology (Sobolev *et al.*, 2007). Although this is certainly indicated by the present analysis (Fig. 9c), the support is conditioned on melt fraction. When the melt fraction of a solid-state stage 2 pyroxenite is high, partial melts will display FeO/MnO ratios that are indistinguishable from those of melts

of peridotite (Fig. 9c). Although not shown, the FeO/MnO of extensively melted stage 2 pyroxenite formed by melt–rock reaction may remain high. It has also been suggested that lavas from Hawaii might have high Fe/Mn because the source is intrinsically high in iron (Humayun *et al.*, 2004). These hypotheses are tested below.

Ni contents

The mixing in of a large amount of basalt will transform a peridotite to a pyroxenite. When the amount of basalt is 35–55% (Fig. 10a) the resultant mixture is coincident in composition with the lower mantle assemblage CaPv + MgPv + CF (Fig. 8). When the amount of basalt is ~50–85%, the mixture is coincident with the upper mantle assemblage Cpx + Gt ± Opx (Fig. 8), and Ni contents are substantially higher than those of peridotite-source melts (Fig. 10a). As discussed below, these Ni-rich stage 2 pyroxenites are likely to be sources that melt and crystallize olivine phenocrysts with high Ni contents. In general, the Ni contents of troctolite and olivine gabbro cumulates of MORB are similar to those of peridotite-source melts, but some are higher in Ni (Fig. 10a).

Whole-rock pyroxenite Ni contents shown in Fig. 10a do not directly constrain the Ni contents of their partial melts and the olivines that would crystallize from these melts. We need to know which minerals define the pyroxenite residues and the following is a short list of possibilities: L + Gt, L + Cpx, L + Opx, L + Gt + Cpx, L + Gt + Cpx + Opx, L + Gt + Cpx + Ol (Longhi, 2002; Herzberg, 2006; Sobolev *et al.*, 2007). For example, the Ni content of a partial melt will be higher than those indicated in Fig. 10a if garnet is the sole residual phase because the partition coefficient of Ni between garnet and liquid, D Ni Gt/L, is <1 (Herzberg & Zhang, 1996; Sobolev *et al.*, 2005). A great deal of experimental work needs to be done to understand how, exactly, Ni partitions amongst liquid and the various crystalline phases and their combinations. However, existing work indicates values of D Ni Ol/L > 1, D Opx/L > 1, D Cpx/L ~ 1 and D Gt/L < 1 (Sobolev *et al.*, 2005). Therefore, partial melts of pyroxenite can have Ni contents that are higher or lower than the whole-rock pyroxenites shown in Fig. 10a. Additionally, most partial melts are expected to have MgO contents that are lower than their pyroxenite source (Sobolev *et al.*, 2007), although there are important exceptions (Herzberg, 2006).

It has been suggested that high-Ni olivines can crystallize from partial melts of eclogite that forms by direct transformation of subducted crust; that is, the stage 1 pyroxenite in Fig. 8 (Wang & Gaetani, 2008). Similarly, high-Ni olivines can crystallize from partial melts of an olivine-free stage 2 pyroxenite that is produced when eclogite partial melts react with peridotite (Sobolev *et al.*, 2005). The later possibility is shown in Fig. 10a. The Ni contents of partial melts of eclogite reported by Pertermann & Hirschmann (2003) were calculated based on the assumption that they equilibrate with peridotite containing olivine with 2828 ppm Ni (Ionov, 2007). The resulting stage 2 pyroxenites will consist of Cpx + Gt ± Opx, and have some of the highest Ni contents of all possible pyroxenites (Fig. 10a).

How will the Ni content of a peridotite-source partial melt be affected by mixing a limited amount of recycled crust into the peridotite during convective stirring? Although not illustrated, it can be shown that addition of 20–30% of a basalt like those illustrated in Fig. 10a has a negligible impact on the Ni content of the partial melts.

Olivine nickel contents from pyroxenite melts

The formation of stage 2 pyroxenites with the Ni contents shown in Fig. 10a can now be used to partially constrain the Ni contents of olivine phenocrysts; the results are shown in Fig. 10b. The constraint is only partial because it was assumed that the stage 2 pyroxenite whole-rock compositions were totally melted. This permitted the olivine composition to be calculated in the usual way, using olivine/liquid Ni distribution coefficients from Beattie *et al.* (1991) together with a 1 atm Fe/Mg exchange coefficient from Toplis (2005). Of course, we really need to know the Ni content of olivine that would crystallize from partial melts of proxenite, not total melts. There are few experimental data on such partial melts, and even fewer data on their Ni contents. As discussed above and shown in Fig. 10a, the Ni contents of partial melts may be greater or less than those of the whole-rock pyroxenites, depending on the mineralogy of the residue. Calculated Ni contents of olivine are expected to vary in a similar manner. Nevertheless, it will be shown below that Fig. 10b probably captures the range of possibilities. The essential observation is that the Ni contents of olivines that crystallize from pyroxenite-source melts can be higher than those of olivines that crystallize from peridotite-source melts (Fig. 10b), in agreement with the conclusions of Sobolev *et al.* (2005). This is further explored for Hawaii.

HIGH-SILICA PYROXENITE SOURCE PARTIAL MELTING BELOW HAWAII

Whole-rock geochemistry of shield-building basalts

An examination is now made of the hypothesis that the shield-building lavas of Hawaii were generated from a pyroxenite source that involved the participation of recycled crust (Hauri, 1996; Lassiter & Hauri, 1998; Blichert-Toft *et al.*, 1999; Huang & Frey, 2005; Huang *et al.*, 2005; Sobolev *et al.*, 2005, 2007; Herzberg, 2006). Whole-rock MgO–CaO data are shown in Fig. 11 for Loihi, Mauna Kea, Kilauea, Mauna Loa and Koolau (Makapuu stage)

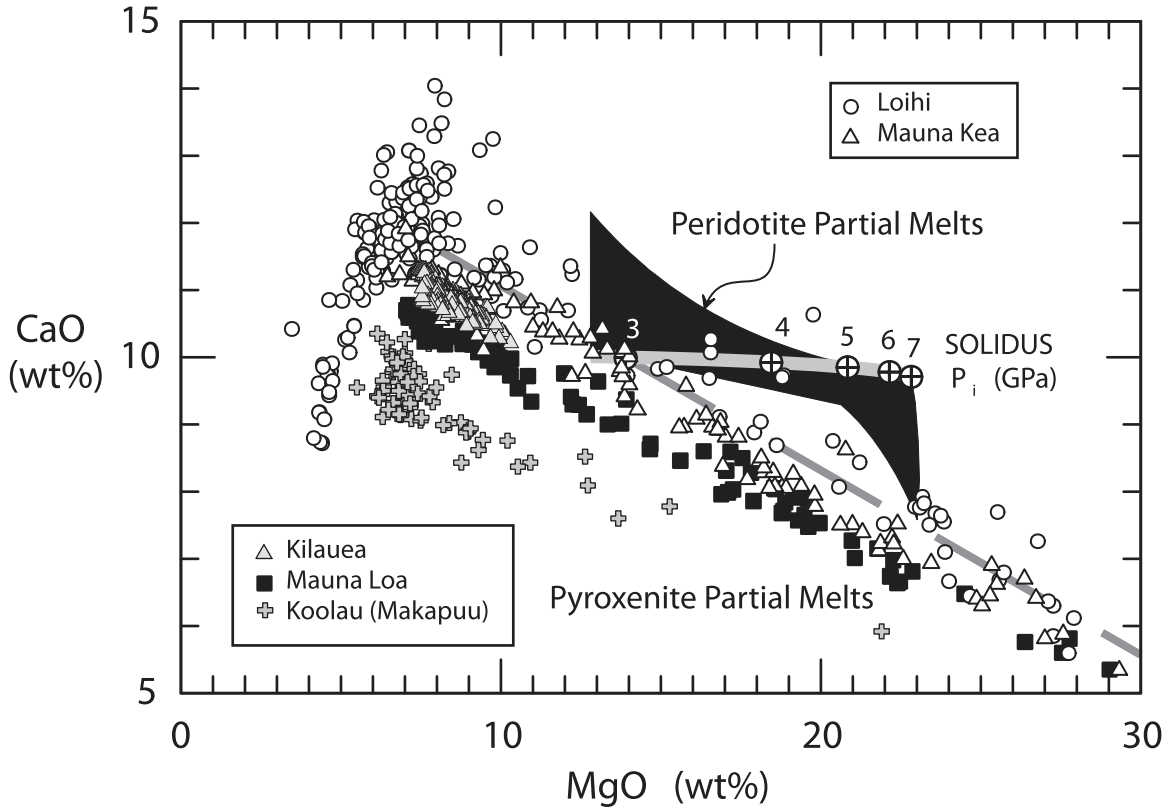

Fig. 11. MgO vs CaO content of lavas from Hawaii. Broken grey line is from Herzberg & Asimow (2008) and separates peridotite- and pyroxenite-source primary magmas. It should be noted that some high-CaO pyroxenite-source magmas are possible (Fig. 9b).

(Moore *et al.*, 1982; Frey & Clague, 1983; Rhodes, 1988, 1995, 1996; Clague *et al.*, 1991; Garcia *et al.*, 1993, 1995, 1998; Frey *et al.*, 1994; Rhodes & Hart, 1995; Norman & Garcia, 1999; Haskins & Garcia, 2004; Rhodes & Vollinger, 2004; Marske *et al.*, 2008). Lavas with MgO > 7–8% exhibit a simple olivine control and at any specified value, 15% for example, CaO is highest for Loihi. Maximum olivine mg-numbers are typically 90–91, and would crystallize from primary magmas with MgO contents in the 15–18% range (Hauri, 1996; Stolper *et al.*, 2004; Herzberg, 2006; Herzberg *et al.*, 2007). With the exception of some lavas from Loihi, most Hawaiian shield-building magmas with 15–18% MgO would have 7–9% CaO, which is lower than those expected from peridotite-source primary magmas formed by accumulated fractional melting (Herzberg, 2006). This is demonstrated in Fig. 11, providing further evidence for the involvement of a pyroxenite source. It should be noted, however, that the CaO contents for peridotite melting were modeled from the experimental results of Walter (1998) on fertile peridotite KR-4003. It is possible that comparable high-quality experiments on other peridotite compositions will yield lower CaO primary magmas, but they have not been reported to date (see also Davis *et al.*, 2009). CaO should remain incompatible during peridotite melting, and partial melts should be elevated in CaO as long as the amount of Cpx is low (Fig. 9b and discussion therein).

Olivine chemistry

Supporting evidence for pyroxenite melting is provided by olivine compositions (Sobolev *et al.*, 2005, 2007), shown in Fig. 12 and Electronic Appendix 3 (http:www.petrology.oupjournals.org). Low whole-rock CaO (Fig. 11) is also revealed in low Ca in olivine (Fig. 12). Olivines are higher in Ni and Fe/Mn and lower in Mn and Ca than those expected of partial melts of a normal peridotite source. Some peridotites may be unusually high in Ni (Fig. 2), but even these are not likely to produce primary magmas that crystallize olivine with 4500 ppm Ni (Fig. 12). Koolau olivines exhibit high Ni even for mg-numbers as low as 86 and, as discussed in detail below, the large spread of mg-numbers is an expected consequence of pyroxenite melting. Batch crystallization (Wang & Gaetani, 2008) can contribute to this spread in mg-number, but this seems unlikely because, by definition, it contributes to phase homogeneity.

With the exception of some olivine phenocrysts from Loihi, most olivines have Mn contents that are lower

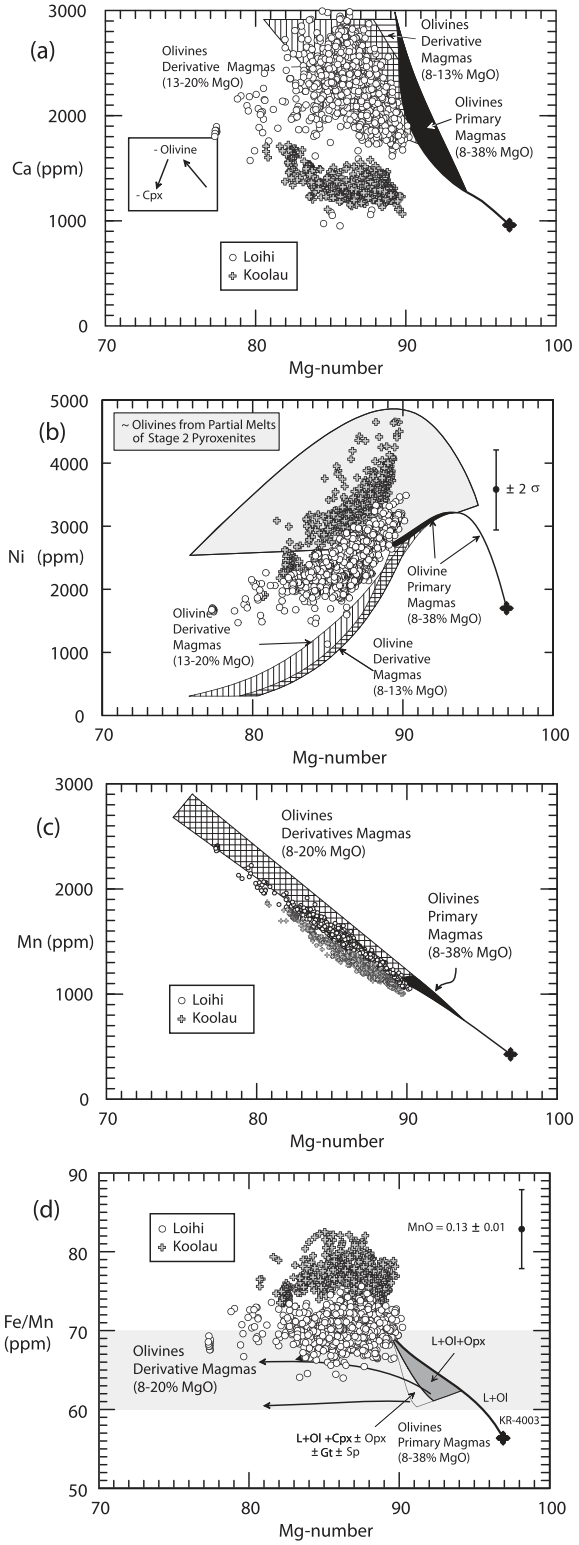

Fig. 12. Calculated olivine phenocryst compositions for melts of a peridotite source compared with observed olivines from Loihi and Koolau volcanoes, Hawaii (Sobolev *et al.*, 2007). (a) High Ca in Loihi olivines reflects the high Ca in the lavas from which they crystallize (Fig. 11). (b) High Ni and the wide range in mg-numbers for Koolau olivines are similar to those expected for olivines from pyroxenite sources. (c) Observed Koolau olivines are generally lower in Mn than those from peridotite sources. (d) Observed Koolau olivines are generally higher in Fe/Mn than those from peridotite sources because Mn is low. In all cases, olivines from Loihi indicate greater participation of peridotite melts than do olivines from Koolau.

than those of peridotite melts and their derivative liquids (Fig. 12c; Electronic Appendix 3). This provides evidence for Mn retention during melt generation in a garnet-rich residue (Fig. 9c). The bulk-rock high Fe/Mn characteristic of Hawaiian lavas (Humayun *et al.*, 2004) is reflected in olivine compositions (Fig. 12d; Electronic Appendix 3). It is inferred that Fe/Mn is high because Mn is low, not because the source is Fe-rich. Therefore, the origin of high Fe/Mn in Hawaii is consistent with pyroxenite-source melting (Sobolev *et al.*, 2007), not Fe enrichment of the source (Humayun *et al.*, 2004).

Sobolev *et al.* (2005) suggested that the olivine phenocryst data can be explained by crystallization from parental magmas that are mixtures of pyroxenite- and peridotite-source melts. The proportion of pyroxenite-derived melt was estimated to be ~90% for Koolau, 60% for Mauna Loa, and 40% for Mauna Kea/Kilauea (Sobolev *et al.*, 2005); more recent calculations yield about 70% pyroxenite for Koolau (A. Sobolev, personal communication). An important phase equilibrium restriction on the mixing of low-SiO_2 peridotite- and high-SiO_2 pyroxenite-source magmas is that it can occur only if they share the same conduit or shallow-level magma chamber. Within the high-pressure melting regime, the garnet–pyroxene plane is a thermal and compositional divide that separates low-SiO_2 peridotite-source magmas to the olivine-rich side from high-SiO_2 pyroxenite-source lavas to the silica-rich side (O'Hara & Yoder, 1967; Milholland & Presnall, 1998; Kogiso *et al.*, 2004; Herzberg, 2006). Any commingling of such magmas must result in pyroxenite precipitation, not magma mixing. The reaction will be low-SiO_2 peridotite melt + high-SiO_2 pyroxenite melt = cpx + gt ± opx. A simple analogue of this reaction can be visualized in Fig. 1 by the reaction of melt X or Y with melt Z to form crystalline pyroxenite. The reaction must proceed until the magma with the lower mass fraction is totally consumed, either the low- or high-SiO_2 magma. Possible examples of such pyroxenites are those that were described by Keshav *et al.* (2007) from Salt Lake Crater in Hawaii.

Olivine compositions from Mauna Kea HSDP2 lavas (Electronic Appendix 3) are similar to those of Koolau and other Hawaiian shield volcanoes; these have also been interpreted to have crystallized from a mixture of pyroxenite- and peridotite-source melts (Sobolev *et al.*, 2007). However, Mauna Kea HSDP2 whole-rock compositions reveal SiO_2-rich and -poor populations with distinctive Zr/Nb and helium isotope compositions (Kurz *et al.*, 2004; Rhodes & Vollinger, 2004; see below). Glasses are even more strongly resolved into separate SiO_2-rich and -poor populations (Stolper *et al.*, 2004; Herzberg, 2006). These SiO_2-rich and -poor lavas have identical NiO and CaO contents (Rhodes & Vollinger, 2004), evidence that does not support variable contributions of melts from

peridotite and pyroxenite. As an alternative to the Sobolev model of mixed peridotite–pyroxenite provenance, it was proposed that these Mauna Kea lavas formed from 100% pyroxenite melts on the high- and low-SiO_2 sides of the pyroxene–garnet plane deep in the mantle, with minimal mixing anywhere (Herzberg, 2006). The 100% pyroxenite model is further explored below as a possible lithological source for the shield-building lavas from Kooalu, Mauna Loa, Mauna Kea, and Kilauea.

Evidence that supports the mixing of peridotite- and pyroxenite-source lavas is revealed by the pre-shield olivines from Loihi (Fig. 12). Compared with the other Hawaiian volcanoes, olivines from Loihi are elevated in Ca and Mn, and low in Ni, trending in the direction expected of olivines from peridotite-source melts. However, an alternative interpretation is that Loihi basalts might be the product of melting from a 100% olivine pyroxenite source, similar to peridotite but with less olivine (see below).

Pyroxenite compositions and primary magmas

The pyroxene–garnet plane (Fig. 13a) has great petrological utility. SiO_2-rich pyroxenites will produce SiO_2-rich melts that project to the SiO_2-rich side of the pyroxene–garnet plane. Similarly, SiO_2-poor rocks will produce SiO_2-poor melts. Given the abundance of evidence from olivine phenocryst compositions in Hawaii for pyroxenite melting, the challenge is to determine how primary magmas can be produced by 100% pyroxenite melting, and whether they are SiO_2-rich or -poor.

As discussed previously (Herzberg, 2006), in all cases primary magma compositions were calculated from primitive lavas that exhibit olivine addition and subtraction. To these samples, olivine was added or subtracted and the calculation was stopped when the liquid reached the cotectics [L + Opx + Cpx + Gt] and [L + Ol + Cpx + Gt], yielding model 100% primary pyroxenite-source magmas. The cotectics shown in Fig. 13 at 3 GPa were calibrated from the experimental data summarized by Herzberg (2006). Cotectics at higher pressures were calibrated from the experimental data of Walter (1998), Yaxley & Sobolev (2007), Sobolev *et al.* (2007), and Spandler *et al.* (2008). Liquids produced by the partial melting of Cpx + Gt + Opx and Cpx + Gt + Ol assemblages will shift towards diopside and away from garnet with increasing pressure (Fig. 13). Pressure information can be inferred from the projection of these liquid compositions to or from olivine into the pyroxene–garnet plane, and a computational algorithm is provided in the caption to Fig. 13b. This pressure is used together with those in Olivine–Cats–Quartz in Fig. 13a to determine when to stop the olivine addition or subtraction in the primary magma calculation, and a computational algorithm is provided in the caption to Fig. 13. It is emphasized that this procedure is tractable only for pyroxenite lithologies that consist of Cpx + Gt + Opx and Cpx + Gt + Ol assemblages. Although primary magma compositions of bimineralic eclogite Cpx + Gt cannot be uniquely constrained, less olivine is added to obtain them. Consequently, model primary magmas for Cpx + Gt + Opx and Cpx + Gt + Ol will provide an upper bound to the MgO contents of most pyroxenite-source magmas. The issue of bimineralic eclogite receives detailed attention below.

Pyroxenite-source primary magma compositions for Koolau project to the SiO_2-rich side of the pyroxene–garnet plane (Fig. 13a and b). Although not shown for the sake of preserving clarity, similar results are obtained for Kooalu, Mauna Kea, and Kilauea. We can infer, therefore, that the Hawaiian source lithology is a SiO_2-rich pyroxenite, consisting of Cpx + Gt + Silica ± Opx. This result is in agreement with the conclusions of Sobolev *et al.* (2005) that the pyroxenite source is olivine-free. Model primary magmas for L + Cpx + Gt + Opx are similar to experimental cotectic melt compositions at ~3·5 GPa. This pressure is consistent with melting below the lithosphere, which is constrained by seismology to be ~100–130 km thick below the big island of Hawaii (Li *et al.*, 2000, 2004). Such high pressures will yield similar primary magma compositions for sources composed of bimineralic eclogite. Lee *et al.* (2009) estimated melting pressures as low as 1·5 GPa, but this result assumes that olivine participates in melting, in contrast to the inference of an olivine-free pyroxenite source here and by Sobolev *et al.* (2005).

Compared with oceanic islands worldwide, Hawaii is unusual in generating melts from a silica-rich pyroxenite source. Silica-poor pyroxenite sources are more common and Loihi is a possible example (Fig. 13). Some Loihi lavas were probably generated from peridotite instead of pyroxenite, as discussed above, and these generally have somewhat higher MgO contents as calculated using the PRIMELT2 software (Herzberg & Asimow, 2008). However, the amount of olivine that is added or subtracted in a primary magma calculation will not affect its position within Fig. 13b, as this is a projection to and from olivine. All Loihi primary magmas plot to the SiO_2-poor side of the thermal divide in Fig. 13b, regardless of uncertainties in peridotite versus pyroxenite provenance. If pyroxenite, however, it can be inferred that the melts were derived from a SiO_2-poor assemblage of Ol + Cpx + Gt and Opx + Cpx + Gt on the low-SiO_2 side of the divide. The relative importance of olivine in the Loihi source is consistent with olivine phenocrysts compositions that have lower Ni (Fig. 12b).

Each Hawaiian volcano displays a range of primary magma compositions; the range of SiO_2 contents is summarized in Fig. 14. The SiO_2 contents of the primary magmas are compared with the approximate SiO_2 content (48·2 wt %) of cotectic liquids in equilibrium with

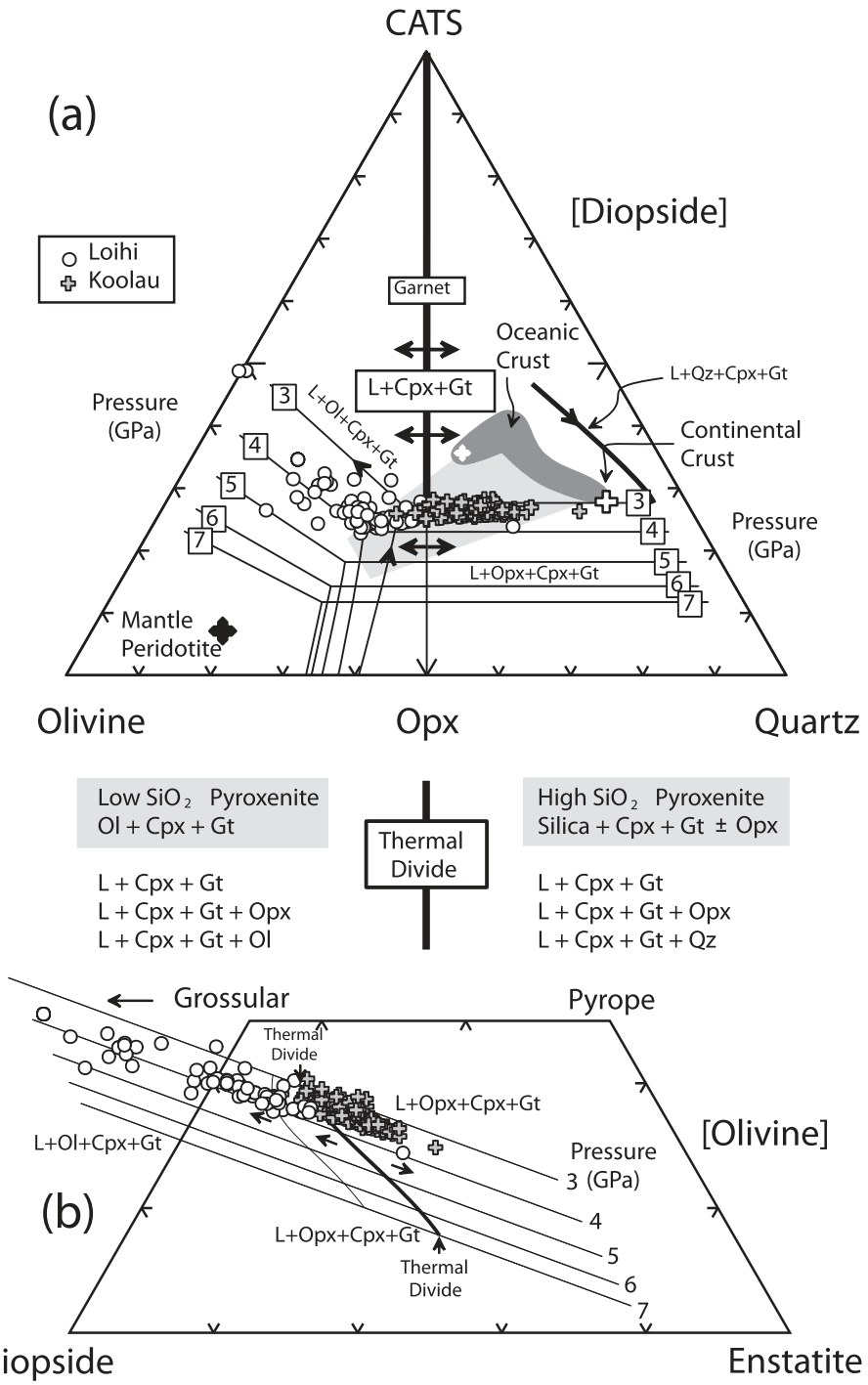

Fig. 13. Projections (mol %) of model pyroxenite-source primary magmas for Loihi and Koolau. (a) Primary magmas from or towards Diopside into the plane Olivine–Quartz–Calcium Tschermak's (CATS). These are calculated by adding and subtracting olivine to lavas that experienced only olivine fractionation, and typically involves lavas with MgO > 7·5% for most shield building lavas from Hawaii. The calculation is stopped when the melt composition is coincident with the cotectic [L + Opx + Cpx + Gt] or [L + Ol + Cpx + Gt] as constrained by the pressure P (GPa) given in (b). Projection coordinates are defined in Fig. 8. For L + Opx + Cpx + Gt on both sides of the thermal divide: $CATS = 0{\cdot}8109P^2 + 61{\cdot}064\ln(P) - 38{\cdot}792[\ln(P)]^2$. For L + Ol + Cpx + Gt: $OL = X - (X - Y)/[(Z)(Z - CATS)]$ where $X = 15{\cdot}0176 + 13{\cdot}9968P - 0{\cdot}77955P^2$, $Y = 4{\cdot}7864 + 8{\cdot}9128P - 0{\cdot}4559P^2$, $Z = 100 - X$. Oceanic crust is from Fig. 8. Continental crust is from Rudnick & Gao (2003). The field indicated in light grey delineates the range of plausible whole-rock pyroxenite source compositions for Hawaii. (b) Primary magmas projected from or towards Olivine into the plane CS–MS–A which is a larger portion of the pyroxene–garnet plane. Projection code is from O'Hara (1968): $CS = CaO + 2(Na_2O + K_2O) - 3{\cdot}333P_2O_5$. $MS = 2SiO_2 + TiO_2 - (FeO + MnO + MgO + NiO) - 2CaO - 8(Na_2O + K_2O) + 6{\cdot}666P_2O_5$. $A = TiO_2 + Al_2O_3 + Cr_2O_3 + Na_2O + K_2O$. Isobaric cotectics can be calculated from: $A = 20{\cdot}188 - 5{\cdot}2595P + 0{\cdot}27P^2 + 0{\cdot}5389CS$. Pressures for all pyroxenite cotectics: $P(GPa) = \exp[1{\cdot}6748 - 0{\cdot}0838(A - 0{\cdot}5389CS)]$. The thermal divide separates low- and high-SiO_2 pyroxenite cotectics [L + Opx + Cpx + Gt] on each side and is described by $MS = 1/\{0{\cdot}00871 + 0{\cdot}02019/A + 0{\cdot}000303[\ln(A)]^3\}$. The curve separating low-SiO_2 pyroxenite cotectics [L + Opx + Cpx + Gt] and the olivine pyroxenite cotectic [L + Ol + Cpx + Gt] is described by $MS = -12{\cdot}5693A + 0{\cdot}21012A^2 + 73{\cdot}8954\ln(A)$.

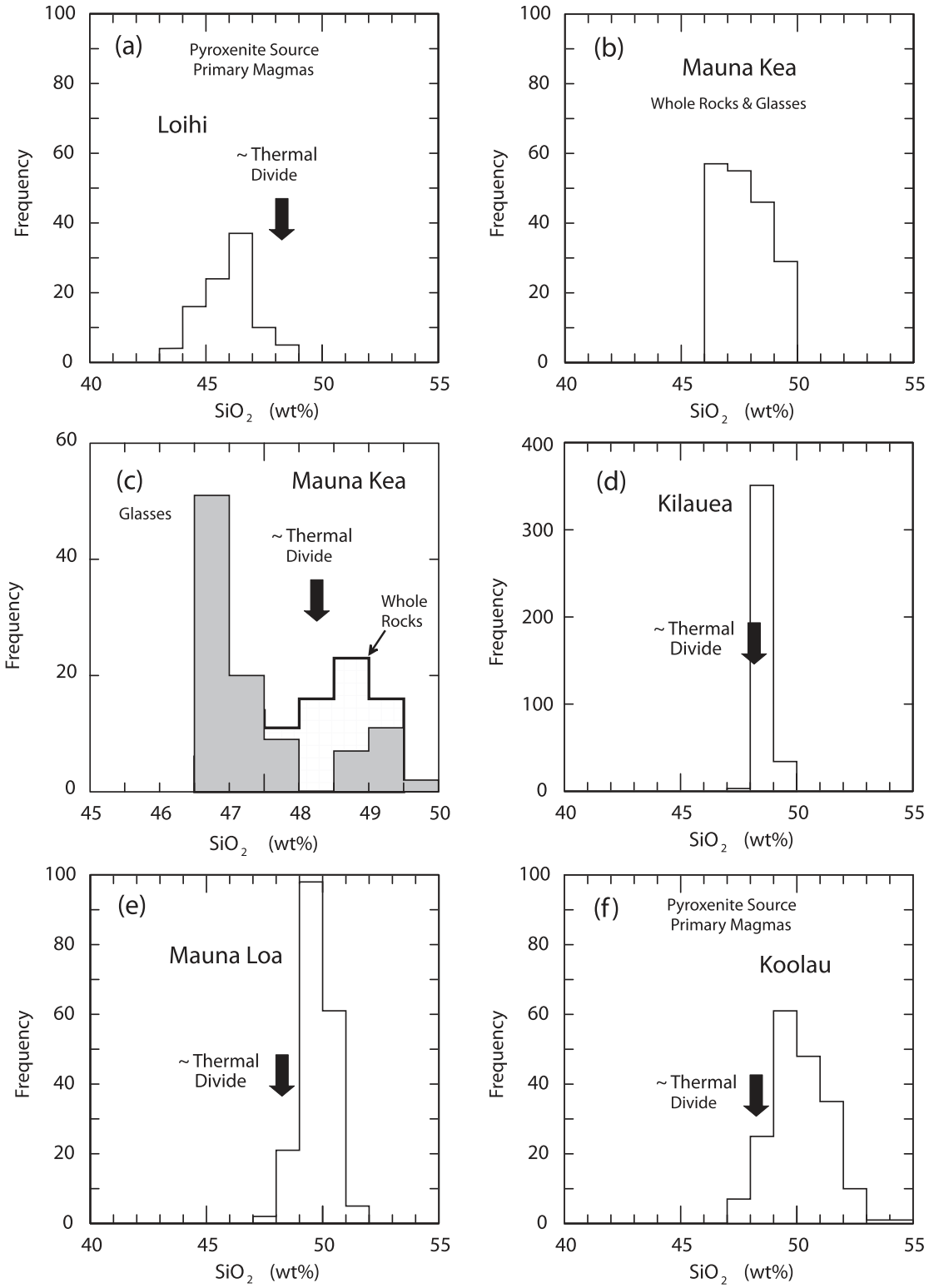

Fig. 14. Summary of SiO_2 contents of model 100% pyroxenite-source primary magmas for Hawaii. Method of calculation is illustrated in Fig. 13. Liquids on L + Cpx + Gt + Opx cotectic nearest the pyroxenite–garnet plane contain ~48·2% SiO_2. SiO_2-rich and -poor type pyroxenites and their partial melts are defined here as having compositions on the SiO_2-rich and -poor sides of the thermal divide, respectively. It should be noted that the two glass populations from Mauna Kea are inferred to define SiO_2-rich and -poor type pyroxenite-source primary magmas (Herzberg, 2006), and there is little or no mixing.

L + Cpx + Gt + Opx near the pyroxene–garnet plane. Partial melting of a SiO_2-rich pyroxenite Cpx + Gt + Silica + Opx will yield liquids on the cotectic L + Cpx + Gt + Opx with $SiO_2 > 48{\cdot}2\%$, as is the case for Kilauea, Mauna Loa, and Koolau volcanoes (Fig. 14d–f). Mauna Kea whole-rock compositions yield SiO_2 contents $> 48{\cdot}2\%$ or $< 48{\cdot}2\%$ (Fig. 14b; Rhodes & Vollinger, 2004); however, electron microprobe analyses of glasses demonstrate a clear separation into SiO_2-rich and -poor primary magma populations (Fig. 14c; Stolper *et al.*, 2004). The evidence from the glasses supports the restriction of magma mixing on a micrometer scale appropriate for electron microprobe analysis. The evidence from the whole-rocks indicates that partial mixing occurs at lower pressures during transit to the surface or within shallow magma chambers; however, even whole-rock Mauna Kea lavas reveal distinct low- and high-SiO_2 populations (Rhodes & Vollinger, 2004; Herzberg, 2006).

The SiO_2 contents of the primary magmas generally increase in the following order: Loihi < Mauna Kea < Kilauea < Mauna Loa < Koolau. The partial melting of SiO_2-rich pyroxenite can yield primary magmas with SiO_2 in the ~48–55% range (Fig. 14) and these can mix freely as they are formed on the SiO_2-rich side of the thermal divide. The SiO_2 contents of primary magmas increase down temperature and along the cotectic L + Cpx + Gt + Opx away from the thermal divide (Fig. 13). It may be inferred, therefore, that the temperature of melting is highest for Kilauea and Mauna Kea. This interpretation would be secure if all volcanoes were fed by melts from the same pyroxenite source composition. However, primary magmas with SiO_2 contents >50% are in much greater abundance at Mauna Loa and Koolau. The implication is that the SiO_2 frequency spectrum is partially controlled by the SiO_2 content of the pyroxenite source; the modal abundance of free quartz or coesite is therefore greatest for Koolau. This is consistent with the suggestion of Huang & Frey (2005) that late Koolau basalts require a large contribution of SiO_2-rich melt from recycled crust. However, those workers suggested that the SiO_2-rich 'dacite' melt formed directly as a partial melt of a stage 1 pyroxenite; a silica-rich stage 2 pyroxenite is also a possibility.

$^{187}Os/^{188}Os$ and $^{3}He/^{4}He$ isotope evidence for pyroxenite melting

Hauri (1996) demonstrated that $^{187}Os/^{188}Os$ correlates with the primary magma SiO_2 content; this is shown in Fig. 15a with an expanded dataset (Bennett *et al.*, 1996, 2000; Hauri & Kurz, 1997; Brandon *et al.*, 1998, 1999; Lassiter & Hauri, 1998; Bryce *et al.*, 2005; Arevalo & McDonough, 2008; Ireland *et al.*, 2009*a*, 2009*b*). It can be inferred that SiO_2-rich primary magmas are most abundant at Koolau volcano because the pyroxenite source contains the greatest amount of unreacted crust manifest mineralogically in quartz- or coesite-bearing, stage 1 pyroxenite. It is stressed that the source for Mauna Loa and Koolau magmas is likely to be heterogeneous with respect to modal free silica, and this might reflect limited reaction of recycled crust with peridotite as shown by equations (5) and (6). This heterogeneous source is expected to give rise to melts that mix; Huang & Frey (2005) presented trace element and isotopic evidence for such a model. Mixing is likely for a variety of pyroxenite-source melts, all of which have $SiO_2 > 48{\cdot}2$ wt %.

Helium isotopic evidence also points to the participation of recycled oceanic crust as shown in Fig. 15b. Based on data reported by Kurz *et al.* (1982, 1983, 1987, 1990, 1995, 2004), Rison & Craig (1983), Staudacher *et al.* (1986), Honda *et al.* (1993) and Ren *et al.* (2009), calculated primary pyroxenite magmas with $SiO_2 > 48\%$ exhibit $^{3}He/^{4}He$ Ra in the 8–20 range, and probably formed by the melting of Cpx + Gt ± Opx + Qz (coesite). In contrast, primary pyroxenite melts with $SiO_2 < 48\%$ have $^{3}He/^{4}He$ Ra in the 20–35 range, and probably formed by the melting of Cpx + Gt + Ol and Cpx + Gt + Opx. Melts in physical contact with both peridotite and an olivine pyroxenite body will be compositionally identical and in equilibrium with Ol + Opx + Cpx + Gt. Such a contact will provide the low-SiO_2 terminus of the cotectic L + Ol + Cpx + Gt + Opx in Fig. 13. Advanced melting of the pyroxenite will eliminate olivine, drive melting up the cotectic L + Cpx + Gt + Opx, and yield low-SiO_2 lavas as shown in Fig. 13c (see also Herzberg, 2006). Lavas from Loihi that exhibit the lowest SiO_2 contents might be melts of peridotite, olivine pyroxenite or both lithologies (L + Ol + Cpx + Gt). The implication is that the Hawaiian plume is structured with regions of SiO_2-rich recycled crust embedded within a matrix of peridotite (Fig. 16; Sobolev *et al.*, 2005; Ren *et al.*, 2009). It is inferred that the low $^{3}He/^{4}He$ component is derived from the recycled crust whereas the high $^{3}He/^{4}He$ comes from the peridotite (see also Farnetani & Hofmann, 2010).

Lithological structure of the Hawaiian plume

Illustrated in Fig. 16 is a lithological model of the Hawaiian plume that is consistent with olivine chemistry and bulk-rock major element geochemistry and also with the helium and osmium isotopic data. It has been suggested that the Hawaiian plume consists of recycled crust stretched into elongated filaments (Farnetani *et al.*, 2002; Abouchami *et al.*, 2005), which can have radial widths of ~10 km (Farnetani & Hofmann, 2010). Such large bodies are consistent with an origin of Hawaiian shield basalts as partial melts of 100% pyroxenite. The petrology of SiO_2-rich and -poor pyroxenites further suggests radial lithological zonation to these bodies (Fig. 16). It is inferred that quartz (coesite) pyroxenite in the core of the plume melts to produce SiO_2-rich melts at Mauna Kea, Kilauea,

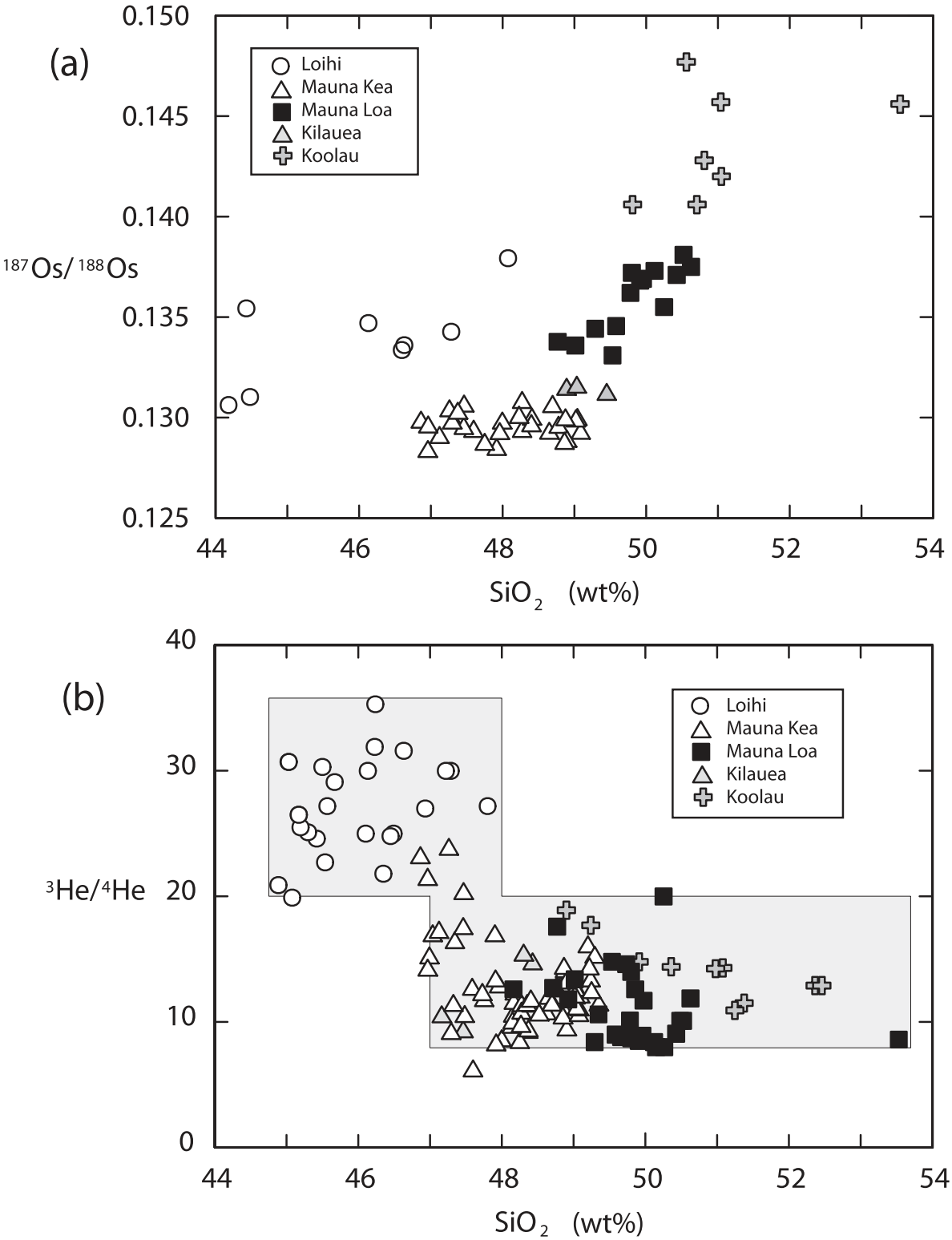

Fig. 15. (a) SiO_2 and osmium isotopic compositions of model 100% pyroxenite-source primary magmas. (b) SiO_2 and helium isotopic compositions of model 100% pyroxenite-source primary magmas. Method of calculation of SiO_2 content of primary magma is illustrated in Fig. 13. Shaded field encompasses all data.

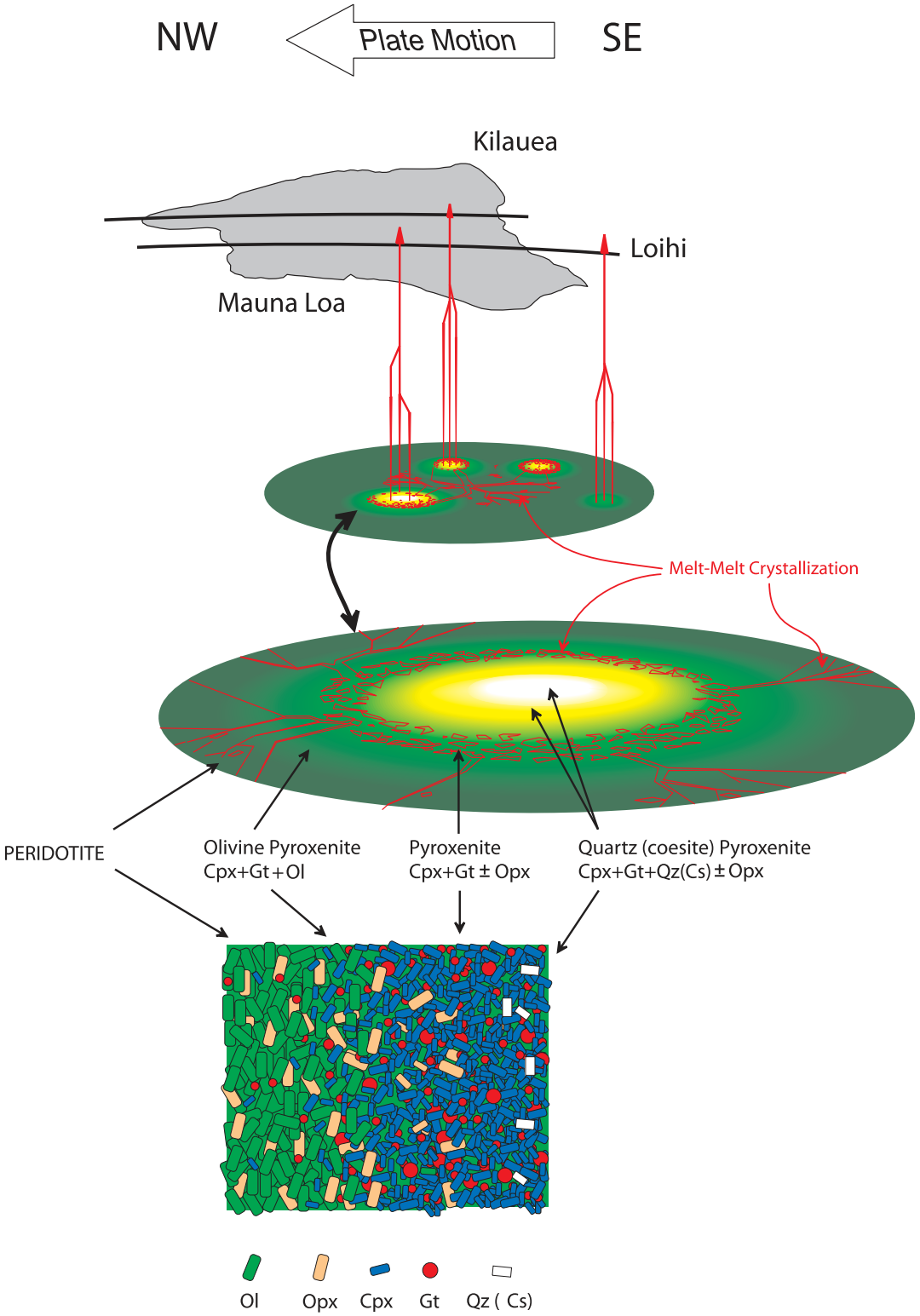

Fig. 16. A model for the lithological structure of the Hawaiian plume in plan view and at scales that range from kilometers (top) to millimeters (bottom). Yellow and white regions contain variable free silica in the source, as quartz (Qz) or coesite (Cs), remnants of silica contained in stage 1 pyroxenite, original recycled crust. Green regions represent stage 2 pyroxenite produced by melt–rock, melt–melt, and/or solid-state reactions, and consist of Cpx + Gt ± Opx. Red markings indicate stage 3 pyroxenite that crystallizes when high-SiO_2 pyroxenite melts interact with low-SiO_2 pyroxenite melts or peridotite melts. Stage 3 pyroxenite is expected to consist of Cpx + Gt ± Opx, similar to stage 2 pyroxenite, and be concentrated between regions of free SiO_2 and olivine. However, stage 3 pyroxenite might also occur in peridotite when high-flux pyroxenite melts flow into the peridotite matrix, which has a lower melt fraction. Although this is depicted in the lateral dimension, both melt–rock and melt–melt reactions are expected to be most prominent in the vertical streamline along which melts ascend. Crystallization is thus likely to be localized at the tops of elongated filaments in a vertical plume conduit, and immediately below the lithosphere where the plume spreads horizontally on impact.

Mauna Loa, and Koolau (Fig. 14c–f). Between the quartz-pyroxenite core and the host peridotite is a peripheral zone of pyroxenite (Cpx + Gt ± Opx), which melts to produce SiO_2-poor primary magmas at Mauna Kea (Fig. 14c). Solid-state mixing of peridotite and peripheral pyroxenite is expected to produce olivine pyroxenite, all of which melt to produce magmas at Loihi (Fig. 14a).

It has been suggested that pyroxenite below Hawaii was formed by the reaction of peridotite with partial melts of recycled oceanic crust (Sobolev *et al.*, 2005). The percolation of such melts within the peridotite matrix is expected to be an efficient way to produce stage 2 pyroxenite. Although it is generally assumed that recycled oceanic crust begins to melt before peridotite, owing to a lower solidus temperature for basaltic compositions (Yasuda *et al.*, 1994; Spandler *et al.*, 2008), peridotite can also begin to melt at high pressure in the presence of CO_2 (Dasgupta & Hirschmann, 2006), producing low-SiO_2 melts (Dasgupta *et al.*, 2007). Low-SiO_2 melts of peridotite might interact with high-SiO_2 melts of recycled crust; such melt–melt reaction may be more common than melt–rock reaction. The intermingling of such melts will trigger crystallization (Figs 1 and 13), not mixing. As discussed above, the reaction of low-SiO_2 peridotite melt + high-SiO_2 pyroxenite melt = Cpx + Gt ± Opx must proceed until the melt with the lower mass fraction is totally consumed, which will be the SiO_2-poor, CO_2-rich peridotite melt. It is suggested here that the peridotite source melts can substantially crystallize to a pyroxenite lithology in this way, possibly yielding rocks that are similar to the xenoliths from Salt Lake Crater on the island of Oahu (Frey, 1980; Sen, 1988; Keshav *et al.*, 2007). This crystallization product, termed a stage 3 pyroxenite, may locally plug the melt pathways, form a sheath around the recycled crust, and act as a permeability barrier that restricts further 'melt–rock' reaction (Fig. 16).

Some peridotite probably occupies the center of the Hawaiian plume (Fig. 16) and it has been proposed that this can melt to produce the high-CaO and -K_2O lavas from Mauna Kea identified by the Hawaii Scientific Drilling Project 2 (HSDP2; Herzberg, 2006). However, in more than 3 km of core, such lavas occupy a small stratigraphic level from 1765 to 1810 m below sea level. Given mantle potential temperatures in the range 1550–1600°C previously estimated for Hawaii (Ribe & Christensen, 1999; Sobolev *et al.*, 2005; Herzberg *et al.*, 2007; Herzberg & Asimow, 2008; Wolfe *et al.*, 2009), the plume is sufficiently hot to melt peridotite. In the model of Sobolev *et al.* (2005, 2007), the peridotite melts mix with pyroxenite melts. In the model proposed in Fig. 16 there is less peridotite and more pyroxenite in the core of the plume and/or peridotite-source melts crystallize to make stage 3 pyroxenite. In contrast, the peripheral part of the plume is dominated by peridotite, not pyroxenite (see also Sobolev *et al.*, 2005), as indicated by Loihi in its present pre-shield stage. This conclusion is also supported by the post-shield lavas from Haleakala, which are high in CaO compared with the shield lavas (http://georoc.mpch-mainz.gwdg.de/georoc/), indicating a switch from shield-stage pyroxenite melting to post-shield peridotite melting. Late Makapuu stage Koolau lavas (Haskins & Garcia, 2004; Huang & Frey, 2005) complicate this interpretation, revealing a strong pyroxenite signature. It is possible that the lithological variability may be laterally asymmetric (Farnetani & Samuel, 2005), especially if the plume conduit is tilted (Wolfe *et al.*, 2009).

Magma productivity in the Hawaiian volcanic chain has generally increased by more than 100% over the past 10 Myr (van Ark & Lin, 2004; Vidal & Bonneville, 2004; Robinson & Eakin, 2006). This might be a reflection of an increase in the amount of recycled crust and a decrease in the amount of peridotite in the plume. However, volume estimates show considerable variability over the past 1 Myr (van Ark & Lin, 2004), and deep pyroxenite crystallization might modulate surface magma productivity.

MgO contents of pyroxenite source primary magmas, and temperatures of melting

A common procedure in petrological modeling is to infer the potential temperature of the mantle source by computing the composition of a primary magma in equilibrium with an assumed mantle olivine composition, or of an olivine composition with a maximum mg-number in a lava flow (e.g. 90). Figure 17 shows the MgO contents of model primary pyroxenite-source magmas of which the SiO_2 contents were illustrated in Fig. 14. The essential feature is that there is no single primary magma composition. Rather, each volcano is constructed from 100% pyroxenite-source primary magmas with a wide range of MgO contents, typically spanning 12–18%. These magmas will crystallize liquidus olivines that are calculated to have mg-numbers in the 86–91 range (Fig. 17), in excellent agreement with the observed olivine compositions (Fig. 12; Electronic Appendix 3). This is in contrast with most petrological models that assume that olivine with a mg-number of 86, is, for example, the sole result of fractional crystallization. The results in Fig. 17 also contrast with models of peridotite melting, in which the MgO contents of the primary magmas and olivine mg-numbers are generally higher.

A fundamental question surrounds the mantle potential temperature that is necessary to produce the range of MgO contents shown in Fig. 17. Unfortunately, there is a lack of experimental data on appropriate pyroxenite

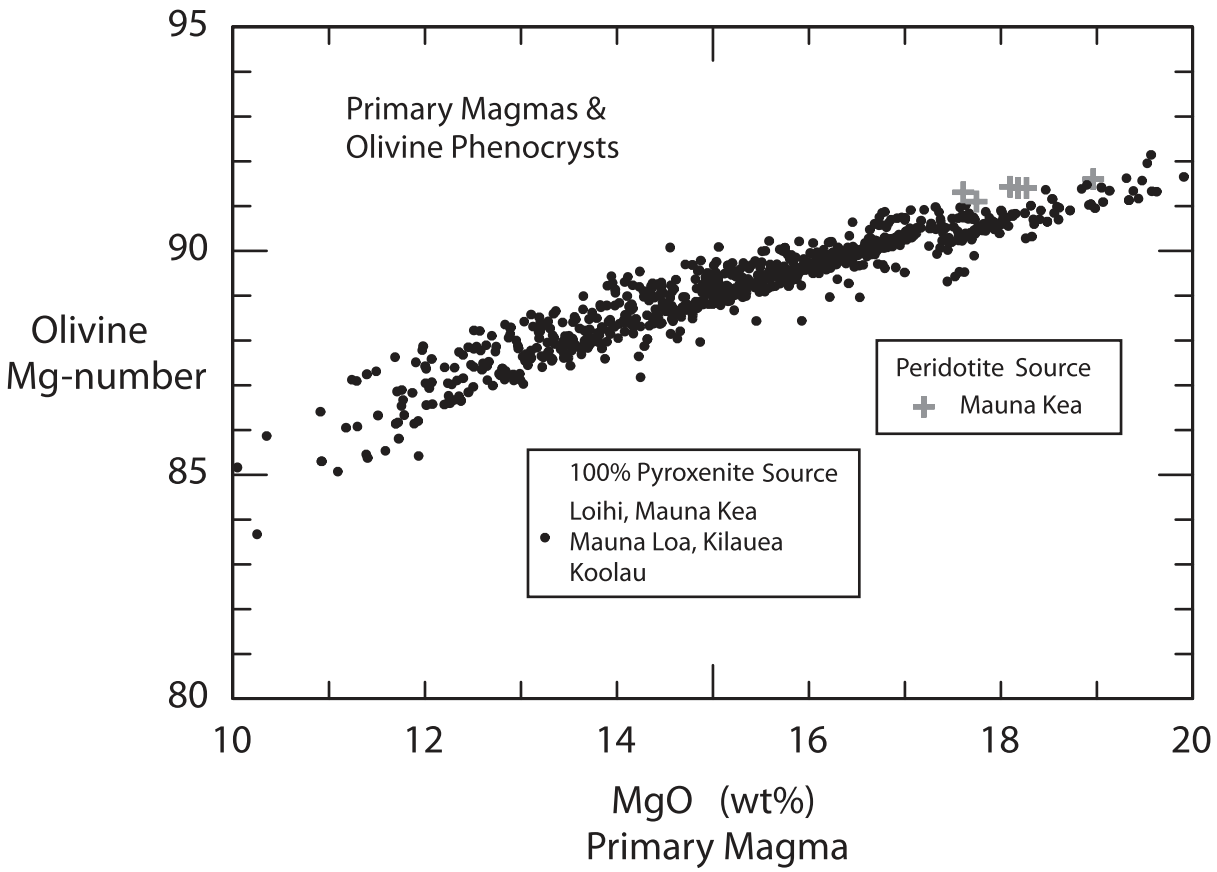

Fig. 17. MgO contents of model peridotite-source and 100% pyroxenite-source primary magmas for Hawaii and the mg-numbers of their crystallizing olivine phenocrysts at the surface.

compositions, so any discussion is conjectural. The available pyroxenite experimental database relevant to Hawaiian lava compositions was reviewed in Herzberg (2006). It is important to stress that few experiments have been performed on compositions similar to those of the model pyroxenite primary magmas. However, existing data suggest that temperatures near the thermal divide are in the range 1560–1580°C at 3 GPa, higher than the 1470–1500°C at the 3 GPa anhydrous peridotite solidus (Herzberg, 2006). Clearly, pyroxenite-source melts can be hotter than peridotite melts, even though they are lower in MgO. The analysis of Mauna Kea lavas is particularly revealing because MgO contents can range from about 13 to 16% for primary pyroxenite-source magmas at the stratigraphic level in the HSDP2 drill core at which high-CaO peridotite-source lavas have been identified (Herzberg, 2006); the latter have 18–19% MgO (Fig. 17). In the absence of any experimental data to the contrary, it is estimated that primary pyroxenite magmas with 13–16% MgO require mantle potential temperatures of 1550–1600°C.

LOW-SILICA PYROXENITE SOURCE MELTING BELOW THE CANARY ISLANDS

Most OIB differ from Hawaii in displaying a more prominent role for nepheline-normative compositions such as trachytes, phonolites, basanites, for which an origin by partial melting of pyroxenite has been proposed (Hirschmann *et al.*, 2003; Kogiso *et al.*, 2003, 2004; Kogiso & Hirschmann, 2006; Dasgupta *et al.*, 2010; Gerbode & Dasgupta, 2010). If it is true that such sources formed from SiO_2-rich recycled oceanic crust, how is it possible to produce SiO_2-poor OIB? The resolution to this paradox might be found in olivine pyroxenite—the expected reaction product between recycled crust and peridotite in the lower mantle [equation (7)]. These pyroxenites have SiO_2-poor compositions; that is, they plot to the SiO_2-poor side of the pyroxene–garnet plane (Figs 8 and 18a). Similarly, cumulate portions of recycled oceanic crust are possible silica-deficient sources. The lithologies for both source possibilities will consist of Ol + Cpx + Gt, and initial melts

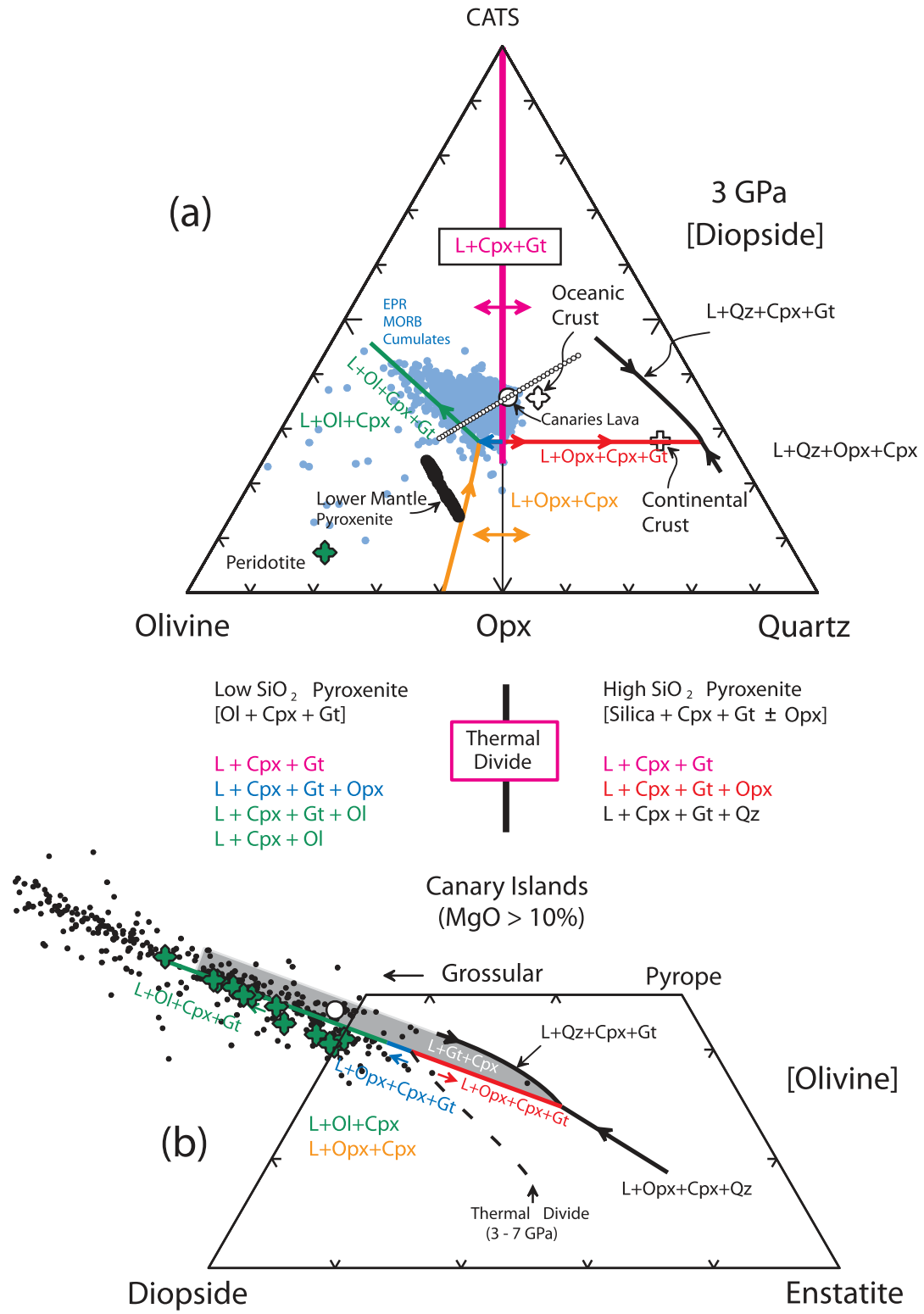

Fig. 18. Phase equilibrium requirements for the production of SiO_2-poor primary OIB from SiO_2-rich recycled crust. (a) A projection of various pyroxenite cotectics (Herzberg, 2006), lower mantle stage 2 olivine pyroxenites and EPR MORB cumulates from or towards Diopside into the plane Olivine–Quartz–Calcium Tschermak's. The large open circle with the array of smaller open circles indicates a whole-rock lava composition from the Canary Islands to (or from) which olivine was added (or subtracted). Oceanic and continental crust compositions are from Herzberg & O'Hara, (2002) and Rudnick & Gao (2003), respectively. (b) A projection of various pyroxenite cotectics (Herzberg, 2006), and whole-rock compositions from or towards Olivine into a part of the pyroxene–garnet plane. This pyroxene–garnet plane is represented as the Opx–CATS line in (a). Black filled circles, primitive lavas from the Canary Islands (GEOROC). Green colored crosses, peridotite-source primary magmas for the Canary Islands (Herzberg & Asimow, 2008). Colored lines are pyroxenite cotectics with the same mineralogy as in (a). The large open circle with the array of smaller open circles indicates a whole-rock lava composition from the Canary Islands to (or from) which olivine was added (or subtracted). The array of smaller open circles is coincident with the large open circle.

will have compositions constrained by the cotectic L + Ol + Cpx + Gt (Fig. 18a). Advanced melts will be defined by L + Ol + Cpx for lower mantle stage 2 pyroxenites and L + Cpx + Gt for the cumulates. The effect of CO_2 is to generate partial melts with even lower SiO_2 contents (Walter *et al.*, 2008; Dasgupta *et al.*, 2010). Addition of CO_2 to SiO_2-rich recycled crust can dilute the amount of SiO_2 and partially contribute to shifting the melt compositions to the SiO_2-poor side of the thermal divide (Gerbode & Dasgupta, 2010).

Primitive lavas from the Canary Islands with MgO > 10% exhibit whole-rock geochemical characteristics that are dominated by olivine addition and subtraction. These have been projected from olivine into the pyroxene–garnet plane in Fig. 18b. It can be seen that the Canary Island lavas mostly project well to the SiO_2-poor side of the thermal divide, in contrast to most SiO_2-rich shield-building lavas from Hawaii (Fig. 13b). Many lavas from the Canary Islands are roughly coincident with the 3 GPa cotectic L + Ol + Cpx + Gt, but there is considerable scatter. The essential question is whether these basalts are melts of peridotite or pyroxenite; Gurenko *et al.* (2009) provided evidence for the involvement of both.

Olivine data (Gurenko *et al.*, 2009) show that many, but not all, lavas from La Gomera are high in Ca and Mn, and low in Ni and Fe/Mn (Electronic Appendix 4), consistent with peridotite melting. Other olivine phenocrysts from La Gomera are shifted systematically in the same general direction as Hawaii, indicating the involvement of recycled crust. Gurenko *et al.* (2009) proposed that the olivines crystallized from partial melts that were mixtures of those from pyroxenite and peridotite lithologies, with increasing amount of pyroxenite in the following order: La Gomera < La Palma < Tenerife < El Heirro. What is most relevant to the present discussion is that partial melts of peridotite can mix freely with those of pyroxenite in the melting region, but only if the pyroxenite source is a low-SiO_2 type, in contrast to Hawaii.

Such mixtures create special difficulties for modeling primary magmas that are calibrated according to criteria for either peridotite or pyroxenite. Results of one such attempt are shown in Fig. 18b. The peridotite-source primary magma compositions for the Canary Islands were estimated from high-CaO primitive lavas (Herzberg & Asimow, 2008; Herzberg & Gazel, 2009), and are shown to be similar to many lavas for which olivine pyroxenite melting is likely. Petrological confusion can arise because both peridotite and olivine pyroxenite partial melts can share common cotectic liquid compositions (L + Ol + Cpx + Gt; Fig. 18a), and mixtures will compromise the primary magma estimates calibrated strictly from peridotite or pyroxenite melting.

Canary Islands data introduce an important note of caution concerning the classification of source pyroxenite types according to whether they are low- or high-SiO_2. Classification is secure as long as a primary magma is saturated in three crystalline phases at the cotectics L + Ol + Cpx + Gt and L + Opx + Cpx + Gt as seen by comparing Fig. 18a and 18b; and most Canary Island basalts appear to be of the low-SiO_2 type. However, let us consider the primitive lava composition indicated by the open circle. Taxonomical information is lost if this lava was formed by melting of a bimineralic eclogite source (L + Cpx + Gt). Addition and subtraction of olivine from such a lava composition can drive compositions to both the low- and high-SiO_2 sides of the pyroxene–garnet plane (Fig. 18a), even though it plots as a low-SiO_2 type in Fig. 18b. The lesson to be drawn is that partial melts of bimineralic eclogite can be either high- or low-SiO_2 types, and there is no clear way to make a petrological distinction.

A final note of caution is warranted. In theory it is possible to calculate the compositions of low-SiO_2 pyroxenite as described above for Hawaii. The danger, however, is that the cotectic L + Ol + Cpx + Gt shown in Fig. 18a has been calibrated from only a few experimental compositions, most of which are low in alkalis. Many OIB are rich in alkalis, H_2O and CO_2, and these are expected to substantially expand and contract the liquidus phase volume of olivine (and orthopyroxene) at the expense of garnet. Unless the effects of pressure and composition can be deconvolved, the result will be a substantial uncertainty in the estimated primary magma MgO content. Compositional effects on the relative stabilities of garnet and clinopyroxene are expected to be less, but these must be checked by experiment.

DISCUSSION

The contents of Ni, Ca, Mn in primary magmas from a normal peridotite source have been constrained using a Jones–Beattie composition-dependent olivine/liquid and orthopyroxene/liquid partitioning model. Normal mantle refers to a pyrolite-like fertile peridotite having 0·25% NiO, 0·13% MnO, 8% FeO and 3·45% CaO. From these, a calculation was made of the compositions of olivine phenocrysts that would crystallize, and the effects of olivine fractionation were evaluated. It is shown that the Ni, Ca, Mn, and Fe/Mn contents of olivine phenocrysts in modern mid-ocean ridge basalts (Sobolev *et al.*, 2007) are consistent with peridotite source melting. Similarly, olivine compositions predicted by the Jones–Beattie method for peridotite melting are in excellent agreement with those of observed olivines in Archean komatiites. These natural laboratory tests illustrate the success of the Jones–Beattie partitioning model in capturing the effects of temperature and pressure.

Olivine phenocrysts in the shield-building lavas on Hawaii are higher in Ni and Fe/Mn, and lower in Mn

and Ca than those expected of a normal peridotite source; they point to the importance of pyroxenite in the source as proposed by Sobolev *et al.* (2005, 2007). Experimental studies indicate that high Fe/Mn in olivine is a consequence of low Mn in the magma sequestered by garnet during partial melting.

There might be multiple origins of the pyroxenite source contributions to intraplate magmatism. Experimental studies rule out the possibility that the pyroxenite is simply unmodified basaltic recycled crust that melts, referred to herein as stage 1 pyroxenite, because the MgO contents of such melts are too low. We are left with three ways to form stage 2 pyroxenite: melt–rock, melt–melt, and rock–rock reaction. The formation of pyroxenite by the reaction of melted subducted oceanic crust with solid peridotite (i.e. melt–rock reaction) was suggested by Sobolev *et al.* (2005). Their model assumes that the recycled crust begins to melt before the peridotite owing to the lower solidus T of basaltic compositions (e.g. Yasuda *et al.*, 1994). However, peridotite can also begin to melt deep in the mantle in the presence of CO_2 (Dasgupta & Hirschmann, 2006), and the intermingling of low-SiO_2 melts of peridotite with high-SiO_2 melts of recycled crust is expected to trigger crystallization (Figs 1 and 13), not mixing—an unusual form of melt–melt reaction. Such crystallization products, herein termed stage 3 pyroxenite, might plug the melt pathways, form a sheath around bodies of recycled crust (Fig. 16), and act as a permeability barrier that restricts further 'melt–rock' reaction. Deep penetration of pyroxenite melts into the surrounding partially melted peridotite will also trigger crystallization and might modulate overall melt productivity.

Stage 2 pyroxenite might also form by solid-state reactions that are expected to occur at the contacts of oceanic crust and peridotite during crustal recycling. The thickness of the solid-state reaction zone is difficult to evaluate. This might be narrow if experimental work on slow volume diffusion is relevant (e.g. Holzapfel *et al.*, 2007). However, the effects of dislocation creep in nature are expected to accelerate solid-state reactions. Recycled crust that has been stretched, thinned and stirred over possibly billions of years might substantially convert to solid-state stage 2 pyroxenite. The possible emplacement in high-temperature lower mantle domains ($T > 2000^{\circ}C$; Ono, 2007) will also accelerate solid-state reactions, especially if CO_2 is present (Dasgupta & Hirschmann, 2006; Collerson *et al.*, 2010; Gerbode & Dasgupta, 2010).

An important issue is whether olivine phenocrysts in Hawaiian basalts crystallized from parental magmas that represent mixtures of partial melts of peridotite and partial melts of pyroxenite (Sobolev *et al.*, 2005, 2007), or from pure pyroxenite melts as suggested in this study. The pyroxene–garnet plane is a high-pressure thermal divide that prohibits the mixing of melts of peridotite and pyroxenite provenance; however, mixing is permitted at lower pressures in melt conduits and crustal magma chambers. Sobolev *et al.* (2005) presented isotopic evidence for such mixing. Data from Mauna Kea, however, reveal low- and high-SiO_2 pyroxenite-source magmas that clearly did not mix. When mixing takes place, an important question is whether it operates on the atomic, micrometer, millimeter, or centimeter scale. Detailed work on olivine-hosted melt inclusions (e.g. Ren *et al.*, 2005) might clarify the mixing issue because the Sobolev model predicts the preservation of melts of diverse peridotite- and pyroxenite-source compositions. In contrast, the 100% pyroxenite model predicts melt inclusion compositions that are similar to the ones modeled here as primary magmas.

Hawaiian shield-stage primary magmas produced by partial melting of a 100% stage 2 pyroxenite contain 12–18% MgO, and would crystallize olivine phenocrysts with mg-numbers in the 86–91 range. Predicted olivine phenocryst compositions in this model are in excellent agreement with those actually observed (Sobolev *et al.*, 2007). Hot pyroxenite sources can yield primary magmas with lower MgO contents than those derived from similarly hot peridotite sources. Primary magmas produced by partial melting of 100% pyroxenite have a range of SiO_2 contents that are positively correlated with $^{187}Os/^{188}Os$ and negatively correlated with $^{3}He/^{4}He$. These are consistent with a Hawaiian plume lithological structure characterized by recycled crust within a peridotite matrix (Sobolev *et al.*, 2005; Ren *et al.*, 2009). Changes in the abundance of stage 2 pyroxenite might be a factor contributing to changes in magma production along the Hawaiian–Emperor volcanic chain.

Pyroxenite bodies that are inferred to be large, as at Hawaii, are expected to contain free SiO_2 that does not completely react out, and these will melt to produce SiO_2-rich magmas. In contrast, free SiO_2 might completely react out in smaller pyroxenite bodies, and form SiO_2-poor olivine pyroxenite in the lower mantle (Figs 8 and 18a). Partial melting of such SiO_2-poor pyroxenite lithologies will produce alkalic basalts in many ocean islands, and the Canary Islands may be representative. Olivine phenocryst compositions from the Canary Islands (Gurenko *et al.*, 2009) are consistent with crystallization of both peridotite- and pyroxenite-source melts that mixed freely. It can be inferred that the bodies of recycled crust in the mantle beneath the Canary Islands are smaller than those in the Hawaiian plume, as revealed by this mixed lithological provenance.

Numerical simulations of solid-state reactions between recycled MORB crust and peridotite mantle reveal that there is likely to be a wide range of whole-rock stage 2 pyroxenite compositions, which will propagate to both their partial melts and crystallizing olivines. The range of possibilites is further enhanced for stage 2 pyroxenites that

might form from ancient oceanic crust that differs from MORB in composition (Herzberg *et al.*, 2010), although these have not been modeled. To this variability we can add a wide range of stage 2 pyroxenite compositions that might form by melt–rock reaction. In all cases variable extents of melting of any stage 2 pyroxenite will add another layer of complexity. It would be remarkable if there is a single pyroxenite end-member that melts to yield magmas that crystallize olivine with a specific and well-defined content of Ni, Mn, Ca, and Fe/Mn. Similarly, there is significant variability in Mn and Fe/Mn in both peridotite partial melts and their olivine phenocrysts (Fig. 6). In general, there are not likely to be well-defined end-member peridotite and pyroxenite sources as proposed by Sobolev *et al.* (2007) and Gurenko *et al.* (2009). Nevertheless, taxonomical difficulties encountered in source lithology identification may yield rich rewards, such as a better understanding of the relationship between lithological diversity in the lower mantle and its petrological expression in intraplate magmatism.

ACKNOWLEDGEMENTS

I am very grateful to many individuals for generously sharing information, data, and ideas. These include: Paul Asimow, Cornelia Class, Raj Dasgupta, Cinzia Farnetani, Mark Feigenson, Mike Garcia, Shan Gao, Esteban Gazel, Al Hofmann, Shichun Huang, Munir Humayun, Matt Jackson, Chusi Li, Yaoling Niu, Zhong-Yuan Ren, and Alex Sobolev. I am especially grateful to Raj Dasgupta, Andrew Greene, and Alex Sobolev for critical reviews, and to Marjorie Wilson for editorial work.

SUPPLEMENTARY DATA

Supplementary data for this paper are available at *Journal of Petrology* online.

REFERENCES

Abouchami, W., Hofmann, A. W., Galer, S. J. G., Frey, F. A., Eisele, J. & Feigenson, M. (2005). Lead isotopes reveal bilateral asymmetry and vertical continuity in the Hawaiian mantle plume. *Nature* **434**, 851–856.

Allègre, C. J. & Turcotte, D. L. (1986). Implications of a two-component marble-cake mantle. *Nature* **323**, 123–127.

Arevalo, R., Jr & McDonough, W. F. (2008). Tungsten geochemistry and implications for understanding the Earth's interior. *Earth and Planetary Science Letters* **272**, 656–665.

Arndt, N. T., Lesher, C. M. & Barnes, S. J. (2008). *Komatiite*. Cambridge: Cambridge University Press, 467 p.

Balta, J. B., Asimow, P. D. & Mosenfelder, J. L. (2010). Manganese partitioning during hydrous melting of peridotite. *Geochimica et Cosmochimica Acta*, in review.

Beattie, P., Ford, C. & Russell, D. (1991). Partition coefficients for olivine–melt and orthopyroxene–melt systems. *Contributions to Mineralogy and Petrology* **109**, 212–224.

Bennett, V. C., East, T. M. & Norman, M. D. (1996). Two mantle-plume components in Hawaiian picrites inferred from correlated Os–Pb isotopes. *Nature* **381**, 221–224.

Bennett, V. C., Norman, M. D. & Garcia, M. O. (2000). Rhenium and platinum group element abundances correlated with mantle source components in Hawaiian picrites: sulphides in the plume. *Earth and Planetary Science Letters* **183**, 513–526.

Berry, A. J., Danyushevsky, D. V., O'Neill, H. St. C., Newville, M. & Sutton, S. R. (2008). Oxidation state of iron in komatiitic melt inclusions indicates hot Archaean mantle. *Nature* **455**, 960–963.

Bézos, A. & Humler, E. (2005). The $Fe^{3+}/\sum Fe$ ratios of MORB glasses and their implications for mantle melting. *Geochimica et Cosmochimica Acta* **69**, 711–725.

Blichert-Toft, J., Frey, F. A. & Albarède, F. (1999). Hf isotope evidence for pelagic sediments in the source of Hawaiian basalts. *Science* **285**, 879–882.

Brandon, A. D., Walker, R. J., Morgan, J. W., Norman, M. D. & Prichard, H. M. (1998). Coupled ^{186}Os and ^{187}Os evidence for core–mantle interaction. *Science* **280**, 1570–1573.

Brandon, A. D., Norman, M. D., Walker, R. J. & Morgan, J. W. (1999). ^{186}Os and ^{187}Os systematics of Hawaiian picrites. *Earth and Planetary Science Letters* **174**, 25–42.

Bryce, J. G., DePaolo, D. J. & Lassiter, J. C. (2005). Geochemical structure of the Hawaiian plume: Sr, Nd, and Os isotopes in the 2·8 km HSDP-2 section of Mauna Kea volcano. *Geochemistry, Geophysics, Geosystems* **6**, GC000809.

Chase, C. G. (1981). Ocean island Pb: Two-stage histories and mantle evolution. *Earth and Planetary Science Letters* **52**, 277–284.

Chauvel, C., Lewin, E., Carpentier, M., Arndt, N. T. & Marini, J. C. (2008). Role of recycled oceanic basalt and sediment in generating the Hf–Nd mantle array. *Nature Geoscience* **1**, 64–67.

Christie, D. M., Carmichael, I. S. E. & Langmuir, C. H. (1986). Oxidation states of mid-ocean ridge basalt glasses. *Earth and Planetary Science Letters* **79**, 397–411.

Clague, D. A., Weber, W. S. & Dixon, J. E. (1991). Picritic glasses from Hawaii. *Nature* **353**, 553–556.

Collerson, K., Williams, Q., Ewart, A. E. & Murphy, D. T. (2010). Origin of HIMU and EM-1 domains sampled by ocean island basalts, kimberlites and carbonatites: The role of CO_2-fluxed lower mantle melting in thermochemical upwellings. *Physics of the Earth and Planetary Interiors* **181**, 112–131.

Dasgupta, R. & Hirschmann, M. M. (2006). Melting in the Earth's deep upper mantle caused by carbon dioxide. *Nature* **440**, 659–662.

Dasgupta, R., Hirschmann, M. M. & Stalker, K. (2006). Immiscible transition from carbonate-rich to silicate-rich melts in the 3 GPa melting interval of eclogite plus CO_2 and genesis of silica-undersaturated ocean island lavas. *Journal of Petrology* **47**, 647–671.

Dasgupta, R., Hirschmann, M. M. & Smith, N. D. (2007). Partial melting experiments of peridotite CO_2 at 3 GPa and genesis of alkalic ocean island basalts. *Journal of Petrology* **48**, 2093–2124.

Dasgupta, R., Jackson, M. G. & Lee, Cin-Ty, A. (2010). Major element chemistry of ocean island basalts—Conditions of mantle melting and heterogeneity of mantle source. *Earth and Planetary Science Letters* **289**, 377–392.

Davis, F. A., Hirschmann, M. M. & Humayun, M. (2009). The composition of low-degree melts of garnet peridotite at 3 GPa by modified iterative sandwich experiments (MISE). *Abstracts, Fall Meeting American Geophysical Union* **90**, V31F–04.

Farnetani, C. G. & Samuel, H. (2005). Beyond the thermal plume paradigm. *Geophysical Research Letters* **32**, doi:10.1029/2005GL022360.

Farnetani, C. G. & Hofmann, A. W. (2010). Dynamics and internal structure of the Hawaiian plume. *Earth and Planetary Science Letters* **295**, 231–240.

Farnetani, C. G., Legras, B. & Tackley, P. J. (2002). Mixing and deformations in mantle plumes. *Earth and Planetary Science Letters* **196**, 1–15.

Frey, F. A. (1980). The origin of pyroxenites and garnet pyroxenites from Salt Lake Crater, Oahu, Hawaii: trace element evidence. *American Journal of Science* **280-A**, 427–449.

Frey, F. A. & Clague, D. A. (1983). Geochemisty of diverse basalt types from Loihi seamount, Hawaii: petrogenetic implications. *Earth and Planetary Science Letters* **66**, 337–355.

Frey, F. A., Garcia, M. O. & Roden, M. F. (1994). Geochemical characteristics of Koolau volcano: implications of intershield geochemical differences among Hawaiian volcanoes. *Geochimica et Cosmochimica Acta* **58**, 1441–1462.

Garcia, M. O., Jorgenson, B. A., Mahoney, J. J., Ito, E. & Irving, A. J. (1993). An evaluation of temporal geochemical evolution of Loihi summit lavas: results from Alvin submersible dives. *Journal of Geophysical Research* **B98**, 537–550.

Garcia, M. O., Foss, D. J. P., West, H. B. & Mahoney, J. J. (1995). Geochemical and isotopic evolution of Loihi volcano, Hawaii. *Journal of Petrology* **36**, 1647–1674.

Garcia, M. O., Rubin, K. H., Norman, M. D., Rhodes, J. M., Graham, D. G., Muenow, D. W. & Spencer, K. J. (1998). Petrology and geochronology of basalt breccia from the 1996 earthquake swarm of Loihi seamount, Hawaii: magmatic history of its 1996 eruption. *Bulletin of Volcanology* **59**, 577–592.

Gerbode, C. & Dasgupta, R. (2010). Carbonated-fluxed melting of MORB-like pyroxenite at 2·9 GPa and genesis of HIMU ocean island basalts. *Journal of Petrology* (in press).

Graham, D. W., Blichert-Toft, J., Russo, C. J., Rubin, K. H. & Albarède, R. (2006). Cryptic striations in the upper mantle revealed by hafnium isotopes in southeast Indian ridge basalts. *Nature* **440**, 199–202.

Green, D. H. & Ringwood, A. E. (1963). Mineral assemblages in a model mantle composition. *Journal of Geophysical Research* **68**, 937–944.

Gurenko, A. A., Sobolev, A. V., Hoernle, K. A., Hauff, F. & Schmincke, H. U. (2009). Enriched, HIMU-type peridotite and depleted recycled pyroxenite in the Canary plume: A mixed-up mantle. *Earth and Planetary Science Letters* **277**, 514–524.

Hart, S. R. & Davis, K. E. (1978). Nickel partitioning between olivine and silicate melt. *Earth and Planetary Science Letters* **40**, 203–219.

Haskins, E. R. & Garcia, M. O. (2004). Scientific drilling reveals geochemical heterogeneity within the Ko'olau shield, Hawai'i. *Contributions to Mineralogy and Petrology* **147**, 162–188.

Hauri, E. H. (1996). Major-element variability in the Hawaiian mantle plume. *Nature* **382**, 415–419.

Hauri, E. H. & Kurz, M. D. (1997). Migration and mantle chromatography, 2: a time-series Os isotope study of Mauna Loa volcano, Hawaii. *Earth and Planetary Science Letters* **153**, 21–36.

Herzberg, C. T. (1993). Lithosphere peridotites of the Kaapvaal craton. *Earth and Planetary Science Letters* **120**, 13–29.

Herzberg, C. (1999). Phase equilibrium constraints on the formation of cratonic mantle. In: Fei, Y., Bertka, C. & Mysen, B. O. (eds) *Mantle Petrology: Field Observations and High Pressure Experimentation: A Tribute to Francis R. (Joe) Boyd. Geochemical Society Special Publication* 6, 241–257.

Herzberg, C. (2004). Geodynamic information in peridotite petrology. *Journal of Petrology* **45**, 2507–2530.

Herzberg, C. (2006). Petrology and thermal structure of the Hawaiian plume from Mauna Kea volcano. *Nature* **444**, 605–609.

Herzberg, C. & Asimow, P. D. (2008). Petrology of some oceanic island basalts: PRIMELT2.XLS software for primary magma calculation. *Geochemistry, Geophysics, Geosystems* **8**, Q09001, doi:10.1029/2008GC002057.

Herzberg, C. & Gazel, E. (2009). Petrological evidence for secular cooling in mantle plumes. *Nature* **458**, 619–622.

Herzberg, C. & O'Hara, M. J. (2002). Plume-associated ultramafic magmas of Phanerozoic age. *Journal of Petrology* **43**, 1857–1883.

Herzberg, C. & Zhang, J. (1996). Melting experiments on anhydrous peridotite KLB-1: Compositions of magmas in the upper mantle and Transition Zone. *Journal of Geophysical Research* **101**, 8271–8295.

Herzberg, C. & Zhang, J. (1998). Melting experiments in the systems $CaO–MgO–Al_2O_3–SiO_2$ and $MgO–SiO_2$ at 3 to 15 GPa. *American Mineralogist* **83**, 491–500.

Herzberg, C., Asimow, P. D., Arndt, N., Niu, Y. L., Lesher, C. M., Fitton, J. G., Cheadle, M. J. & Saunders, A. D. (2007). Temperatures in ambient mantle and plumes: Constraints from basalts, picrites, and komatiites. *Geochemistry, Geophysics, Geosystems* **8**, Q02006, doi:10.1029/2006GC001390.

Herzberg, C., Condie, K. & Korenaga, J. (2010). Thermal history of the Earth and its petrological expression. *Earth and Planetary Science Letters* **292**, 79–88.

Hirose, K. (2006). Postperovskite phase transition and its geophysical implications. *Reviews of Geophysics* **44**, RG3001.

Hirose, K., Takafuji, N., Sata, N. & Ohishi, Y. (2005). Phase transition and density of subducted MORB crust in the lower mantle. *Earth and Planetary Science Letters* **237**, 239–251.

Hirschmann, M. M. & Stolper, E. M. (1996). A possible role for garnet pyroxenite in the origin of the 'garnet signature' in MORB. *Contributions to Mineralogy and Petrology* **124**, 185–208.

Hirschmann, M. M., Kogiso, T., Baker, M. B. & Stolper, E. M. (2003). Alkalic magmas generated by partial melting of garnet pyroxenite. *Geology* **31**, 481–484.

Hofmann, A. W. & White, W. M. (1982). Mantle plumes from ancient oceanic crust. *Earth and Planetary Science Letters* **57**, 421–436.

Holzapfel, C., Chakraborty, S., Rubie, D. D. & Frost, D. J. (2007). Effect of pressure on Fe–Mg, ni and Mn diffusion in $(Fe_XMg_{1-X})_2SiO_4$ olivine. *Physics of the Earth and Planetary Interiors* **162**, 186–198.

Honda, M., McDougall, I., Patterson, D. B., Doulgeris, A. & Clague, D. A. (1993). Noble gases in submarine pillow glasses from Loihi and Kilauea, Hawaii: a solar component in the Earth. *Geochemica et Cosmochimica Acta* **57**, 859–874.

Huang, S. & Frey, F. A. (2005). Recycled oceanic crust in the Hawaiian plume: evidence from temporal geochemical variations within the Koolau shield. *Contributions to Mineralogy and Petrology* **149**, 556–575.

Huang, S., Frey, F., Blichert-Toft, J., Fodor, R. V., Bauer, G. R. & Xu, G. (2005). Enriched components in the Hawaiian plume: Evidence from Kahoolawe volcano, Hawaii. *Geochemistry, Geophysics, Geosystems* **6**, doi:10.1029/2005GC001012.

Humayun, M., Qin, L. P. & Norman, M. D. (2004). Geochemical evidence for excess iron in the mantle beneath Hawaii. *Science* **306**, 91–94.

Ionov, D. A. (2007). Composition variations and heterogeneity in fertile lithospheric mantle: peridotite xenoliths in basalts from Tariat, Mongolia. *Contributions to Mineralogy and Petrology* **154**, 455–477.

Ionov, D. A. & Hofmann, A. W. (2007). Depth of formation of subcontinental off-craton peridotites. *Earth and Planetary Science Letters* **261**, 620–634.

Ireland, T. J., Walker, R. J. & Garcia, M. O. (2009*a*). Highly siderophile element and ^{187}Os isotope systematics of Hawaiian picrites: implications for parental melt composition and source heterogeneity. *Chemical Geology* **260**, 112–128.

Ireland, T. J., Arevalo, R., Jr, Walker, R. J. & McDonough, W. F. (2009*b*). Tungsten in Hawaiian picrites: a compositional model for the sources of Hawaiian lavas. *Geochimica et Cosmochimica Acta* **73**, 4517–4530.

Irifune, T. & Ringwood, A. E. (1993). Phase transformations in subducted oceanic crust and buoyancy relationships at depths of 600–800 km in the mantle. *Earth and Planetary Science Letters* **117**, 101–110.

Irving, A. J. (1980). Petrology and geochemistry of composite ultramafic xenoliths in alkalic basalts and implications for magmatic processes within the mantle. *American Journal of Science* **280-A**, 389–426.

Jackson, M. G. & Dasgupta, R. (2008). Compositions of HIMU, EM1, and EM2 from global trends between radiogenic isotopes and major elements in ocean island basalts. *Earth and Planetary Science Letters* **276**, 175–186.

Jackson, M. G., Hart, S. R., Saal, A. E., Shimizu, N., Kurz, M. D., Blusztajn, J. S. & Skovgaard, A. C. (2008). Globally elevated titanium, tantalum, and niobium (TITAN) in ocean island basalts with high $^{3}He/^{4}He$. *Geochemistry, Geophysics, Geosystems* **9**, Q04027, doi:10.1029/2007GC001876.

Jones, J. H. (1984). Temperature and pressure-independent correlations of olivine–liquid partition coefficients and their application to trace element partitioning. *Contributions to Mineralogy and Petrology* **88**, 126–132.

Kato, T. & Kumazawa, M. (1985). Effect of high pressure on the melting relation in the system Mg_2SiO_4–$MgSiO_3$ Part I. Eutectic relation up to 7 GPa. *Journal of Physics of the Earth* **33**, 513–524.

Kelemen, P. B., Hart, S. R. & Bernstein, S. (1998). Silica enrichment in the continental upper mantle via melt/rock reaction. *Earth and Planetary Science Letters* **164**, 387–406.

Kelley, K. & Cottrell, E. (2009). Water and the oxidation state of subduction zone magmas. *Science* **325**, 605–607.

Keshav, S., Gudfinnsson, G. H., Sen, G. & Fei, Y.-W. (2004). High-pressure melting experiments on garnet clinopyroxenite and the alkalic to tholeiitic transition in ocean-island basalts. *Earth and Planetary Science Letters* **223**, 365–379.

Keshav, S., Sen, G. & Presnall, D. C. (2007). Garnet-bearing xenoliths from Salt Lake Crater, Oahu, Hawaii: high-pressure fractional crystallization in the oceanic mantle. *Journal of Petrology* **48**, 1681–1724.

Kinzler, R. J., Grove, T. L. & Recca, S. I. (1990). An experimental study on the effect of temperature and melt composition on the partitioning of nickel between olivine and silicate melt. *Geochimica et Cosmochimica Acta* **54**, 1255–1265.

Kogiso, T. & Hirschmann, M. M. (2006). Partial melting experiments of bimineralic eclogite and the role of recycled mafic oceanic crust in the genesis of ocean island basalts. *Earth and Planetary Science Letters* **249**, 188–199.

Kogiso, T., Hirschmann, M. M. & Frost, D. J. (2003). High-pressure partial melting of garnet pyroxenite: possible mafic lithologies in the source of ocean island basalts. *Earth and Planetary Science Letters* **216**, 603–617.

Kogiso, T., Hirschmann, M. M. & Pertermann, M. (2004). High-pressure partial melting of mafic lithologies in the mantle. *Journal of Petrology* **45**, 2407–2422.

Kurz, M. D., Jenkins, W. J. & Hart, S. R. (1982). Helium isotopic systematics of oceanic islands and mantle heterogeneity. *Nature* **297**, 42–47.

Kurz, M. D., Tatsumoto, M., Hart, S. R. & Clague, D. A. (1983). Helium isotopic variations in volcanic rocks from Loihi seamount and the island of Hawaii. *Earth and Planetary Science Letters* **66**, 388–406.

Kurz, M. D., Garcia, M. O., Frey, F. A. & O'Brien, P. A. (1987). Temporal helium isotope variations within Hawaiian volcanoes: basalts from Mauna Loa and Haleakala. *Geochimica et Cosmochimica Acta* **51**, 2905–2914.

Kurz, M. D., Colodner, D., Trull, T. W., Moore, R. B. & O'Brien, P. A. (1990). Cosmic ray exposure dating with *in situ* produced cosmogenic ^{3}He: results from young Hawaiian lava flows. *Earth and Planetary Science Letters* **97**, 177–189.

Kurz, M. D., Kenna, T. C., Kammer, D. P., Rhodes, J. M. & Garcia, M. O. (1995). Isotopic evolution of Mauna Loa volcano: a view from the submarine southwest rift zone. In: Rhodes, J. M. & Lockwood, J. P. (eds) *Mauna Loa Revealed. Geophysical Monograph, American Geophysical Union* **92**, 289–306.

Kurz, M. D., Curtice, J. M., Lott, D. E., III & Solow, A. (2004). Rapid helium isotopic variability in Mauna Kea shield lavas from the Hawaiian Scientific Drilling Project. *Geochemistry, Geophysics, Geosystems* **5**, GC000439.

Langmuir, C. H., Klein, E. M. & Plank, T. (1992). Petrology systematics of mid-ocean ridge basalts: constraints on melt generation beneath ocean ridges. In: Morgan, J. P., Blackman, D. K. & Sinton, J. M. (eds) *Mantle Flow and Melt Generation at Mid-Ocean Ridges. Geophysical Monograph, American Geophysical Union* **71**, 183–280.

Lassiter, J. C. & Hauri, H. (1998). Osmium-isotope variations in Hawaiian lavas: evidence for recycled oceanic lithosphere in the Hawaiian plume. *Earth and Planetary Science Letters* **164**, 483–496.

Lee, C.-T., Luffi, P., Plank, T., Dalton, H. & Leeman, W. P. (2009). Constraints on the depths and temperatures of basaltic magma generation on Earth and other terrestrial planets using new thermobarometers for mafic magmas. *Earth and Planetary Science Letters* **279**, 20–33.

Li, C. & Ripley, E. M. (2010). The relative effects of composition and temperature on olivine–liquid Ni partitioning: Statistical deconvolution and implications for petrologic modeling. *Chemical Geology* **275**, 99–104.

Li, X., Kind, R., Priestley, K., Sobolev, S. V., Tilmann, F., Yuan, X. & Weber, M. (2000). Mapping the Hawaiian plume conduit with converted seismic waves. *Nature* **405**, 938–941.

Li, X., Kind, R., Yuan, X., Wölbern, I. & Hanka, W. (2004). Rejuvenation of the lithosphere by the Hawaiian plume. *Nature* **427**, 827–829.

Liu, Y., Gao, S., Kelemen, P. B. & Xu, W. (2008). Recycled crust controls contrasting source compositions of Mesozoic and Cenozoic basalts in the North China Craton. *Geochimica et Cosmochimica Acta* **72**, 2349–2376.

Longhi, J. (2002). Some phase equilibrium systematics of lherzolite melting: I. *Geochemistry, Geophysics, Geosystems* **3**, doi:10.1029/2001GC000204.

Marske, J. P., Garcia, M. O., Pietruszka, A. J., Rhodes, J. M. & Norman, M. D. (2008). Geochemical variations during Kilauea's Pu'u 'O'o eruption reveal a fine-scale mixture of mantle heterogeneities within the Hawaiian plume. *Journal of Petrology* **49**, 1297–1318.

McDonough, W. F. & Sun, S.-s. (1995). The composition of the Earth. *Chemical Geology* **120**, 223–253.

Milholland, C. S. & Presnall, D. C. (1998). Liquidus phase relations in the CaO–MgO–Al_2O_3–SiO_2 system at 3·0 GPa: The aluminous pyroxene thermal divide and high pressure fractionation of picritic and komatiitic magmas. *Journal of Petrology* **39**, 3–27.

Moore, J. G., Clague, D. & Normark, W. R. (1982). Diverse basalt types from Loihi seamount, Hawaii. *Geology* **10**, 88–92.

Niu, Y. & O'Hara, M. J. (2003). Origin of ocean island basalts: a new perspective from petrology, geochemistry, and mineral physics considerations. *Journal of Geophysical Research* **108**, B4, 2209.

Norman, M. D. & Garcia, M. O. (1999). Primitive magmas and source characteristics of the Hawaiian plume: petrology and geochemistry of shield picrites. *Earth and Planetary Science Letters* **168**, 27–44.

O'Hara, M. J. (1967). Mineral facies in ultrabasic rocks. In: Wyllie, P. J. (ed.) *Ultramafic and Related Rocks*. New York: Wiley, pp. 7–17.

O'Hara, M. J. (1968). The bearing of phase equilibria studies in synthetic and natural systems on the origin of basic and ultrabasic rocks. *Earth-Science Reviews* **4**, 69–133.

O'Hara, M. J. & Yoder, H. S., Jr (1967). Formation and fractionation of basic magmas at high pressures. *Scottish Journal of Geology* **3**, 67–117.

Ono, S. (2007). Experimental constraints on the temperature profile in the lower mantle. *Physics of the Earth and Planetary Interiors* **170**, 267–273.

Ono, S., Ito, E. & Katsura, T. (2001). Mineralogy of subducted basaltic crust (MORB) from 25 to 37 GPa, and chemical heterogeneity of the lower mantle. *Earth and Planetary Science Letters* **190**, 57–63.

Pertermann, M. & Hirschmann, M. M. (2003). Anhydrous partial melting experiments on MORB-like eclogite: phase relations, phase compositions and mineral–melt partitioning of major elements at 2–3 GPa. *Journal of Petrology* **44**, 2173–2201.

Pilet, S., Baker, M. B. & Stolper, E. M. (2008). Metasomatized lithosphere and the origin of alkaline lavas. *Science* **320**, 916–919.

Puchtel, I. S., Humayun, M., Campbell, A. J., Sproule, R. A. & Lesher, C. M. (2004). Platinum group element geochemistry of komatiites from the Alexo and Pyke Hill areas, Ontario, Canada. *Geochimica et Cosmochimica Acta* **68**, 1361–1383.

Puchtel, I. S., Walker, R. J., Brandon, A. D. & Nisbet, E. G. (2009). Pt–Re–Os and Sm–Nd isotope and HSE and REE systematics of the 2·7 Ga Belingwe and Abitibi komatiites. *Geochimica et Cosmochimica Acta* **73**, 6367–6389.

Putirka, K. D. (2005). Mantle potential temperatures at Hawaii, Iceland, and the mid-ocean ridge system, as inferred from olivine phenocrysts: Evidence for thermally driven mantle plumes. *Geochemistry, Geophysics, Geosystems* **6**, doi:10.1029/2005GC000915.

Qin, L. & Humayun, M. (2008). The Fe/Mn ratio in MORB and OIB determined by ICP-MS. *Geochimica et Cosmochimica Acta* **72**, 1660–1677.

Ren, Z.-Y., Ingle, S., Takahashi, E., Hirano, N. & Hirata, T. (2005). The chemical structure of the Hawaiian plume. *Nature* **436**, 837–840.

Ren, Z.-Y., Hanyu, T., Miyazaki, T., Chang, Q., Kawabata, H., Takahashi, T., Hirahara, Y., Nichols, R. L. & Tatsumi, Y. (2009). Geochemical differences of the Hawaiian shield lavas: implications for melting processes in the heterogeneous Hawaiian plume. *Journal of Petrology* **50**, 1553–1573.

Rhodes, J. M. (1988). Geochemistry of the 1984 Mauna Loa eruption: implications for magma storage and supply. *Journal of Geophysical Research* **B93**, 4453–4466.

Rhodes, J. M. (1995). The 1852 and 1868 Mauna Loa picrite eruptions: clues to parental magma compositions and the magmatic plumbing system. In: Rhodes, J. M. & Lockwood, J. P. (eds) *Mauna Loa Revealed: Structure, Composition, History and Hazards. Geophysical Monograph, American Geophysical Union* **92**, 241–262.

Rhodes, J. M. (1996). Geochemical stratigraphy of lava flows sampled by the Hawaii Scientific Drilling Project. *Journal of Geophysical Research* **101**, 11729–11746.

Rhodes, J. M. & Hart, S. R. (1995). Episodic trace element and isotopic variations in historical Mauna Loa lavas: implications for magma and plume dynamics. In: Rhodes, J. M. & Lockwood, J. P. (eds) *Mauna Loa Revealed: Structure, Composition, History and Hazards. Geophysical Monograph, American Geophysical Union* **92**, 263–288.

Rhodes, J. M. & Vollinger, M. J. (2004). Composition of basaltic lavas sampled by phase-2 of the Hawaii Scientific Drilling Project: Geochemical stratigraphy and magma types. *Geochemistry, Geophysics, Geosystems* **5**, doi:10.1029/2002GC000434.

Ribe, N. M. & Christensen, U. R. (1999). The dynamical origin of Hawaiian volcanism. *Earth and Planetarey Science Letters* **171**, 517–531.

Rison, W. & Craig, H. (1983). Helium isotopes and mantle volatiles in Loihi seamount and Hawaiian island basalts and xenoliths. *Earth and Planetary Science Letters* **66**, 407–426.

Robinson, J. E. & Eakin, B. W. (2006). Calculated volumes of individual shield volcanoes at the young end of the Hawaiian Ridge. *Journal of Volcanology and Geothermal Research* **151**, 309–317.

Rudnick, R. L. & Gao, S. (2003). The composition of the continental crust. In: Holland, H. D. & Turekian, K. K. (eds) *The Crust, Treatise on Geochemistry 3*. Oxford: Elsevier–Pergamon, pp. 1–64.

Salters, V. J. M., Longhi, J. E. & Bizimis, M. (2002). Near mantle solidus trace element partitioning at pressures up to 3·4 GPa. *Geochemistry, Geophysics, Geosystems* **3**, doi:10.1029/2001GC000148.

Schulze, D. J. (1989). Constrains of abundance of eclogite in the upper mantle. *Journal of Geophysical Research* **94**, 4205–4212.

Sen, G. (1988). Petrogenesis of spinel lherzolite and pyroxenite suite xenoliths from the Koolau shield, Oahu, Hawaii: Implications for petrology of the post-eruptive lithosphere beneath Oahu. *Contributions to Mineralogy and Petrology* **100**, 61–91.

Sobolev, A. V., Hofmann, A. W. & Nikogosian, I. K. (2000). Recycled oceanic crust observed in 'ghost plagioclase' within the source of Mauna Loa lavas. *Nature* **404**, 986–989.

Sobolev, A. V., Hofmann, A. W., Sobolev, S. V. & Nikogosian, I. K. (2005). An olivine-free mantle source of Hawaiian shield basalts. *Nature* **434**, 590–597.

Sobolev, A. V., Hofmann, A. W., Kuzmin, D. V., Yaxley, G. M., Arndt, N. T., Chung, S.-L., Danyushevsky, L. V., Elliott, T., Frey, F. A., Garcia, M. O., Gurenko, A. A., Kamenetsky, V. S., Kerr, A. C., Krivolutskaya, N. A., Matvienkov, V. V., Nikogosian, I. K., Rocholl, A., Sigurdsson, I. A., Sushchevskaya, N. M. & Teklay, M. (2007). The amount of recycled crust in sources of mantle-derived melts. *Science* **316**, 412–417.

Spandler, C., Yaxley, G., Green, D. H. & Rosenthal, A. (2008). Phase relations and melting of anhydrous K-bearing eclogite from 1200 to 1600°C and 3 to 5 GPa. *Journal of Petrology* **49**, 771–795.

Staudacher, T., Kurz, M. D. & Allègre, C.-J. (1986). New noble gas data on glass samples from Loihi seamount and Hualalai and on dunite samples from Loihi and Reunion island. *Chemical Geology* **56**, 193–205.

Stolper, E., Sherman, S., Garcia, M., Baker, M. & Seaman, C. (2004). Glass in the submarine section of the HSDP2 drill core, Hilo, Hawaii. *Geochemistry, Geophysics, Geosystems* **5**, doi:10.1029/2003GC000553.

Straub, S. M., LaGatta, A. B., Pozzo, A. L. M.-D. & Langmuir, C. H. (2008). Evidence from high Ni olivines for a hybridized peridotite/pyroxenite source for orogenic andesites from the central Mexican Volcanic Belt. *Geochemistry, Geophysics, Geosystems* **9**, Q03007, doi:10.1029GC001583.

Toplis, M. J. (2005). The thermodynamics of iron and magnesium partitioning between olivine and liquid: criteria for assessing and predicting equilibrium in natural and experimental systems. *Contributions to Mineralogy and Petrology* **149**, 22–39.

Van Ark, E. & Lin, J. (2004). Time variation in igneous volume flux of the Hawaii–Emperor hot spot seamount chain. *Journal of Geophysical Research* **109**, B11401, doi:10.1029/2003JB002949.

Van Keken, P. & Zhong, S. (1999). Mixing in a 3D spherical model of present-day mantle convection. *Earth and Planetary Science Letters* **171**, 533–547.

Vidal, V. & Bonneville, A. (2004). Variations of the Hawaiian hot spot activity revealed by variations in the magma production rate. *Journal of Geophysical Research* **109**, B03104, doi:10.1029/2003JB002559.

Walter, M. J. (1998). Melting of garnet peridotite and the origin of komatiite and depleted lithosphere. *Journal of Petrology* **39**, 29–60.

Walter, M. J., Bulanova, G. P., Armstrong, L. S., Keshav, S., Blundy, J. D., Gudfinnsson, G., Lord, O. T., Lennie, A. R., Clark, S. M., Smith, C. B. & Gobbo, L. (2008). Primary carbonatite melt from deeply subducted oceanic crust. *Nature* **454**, 622–625.

Wang, Z. & Gaetani, G. A. (2008). Partitioning of Ni between olivine and siliceous eclogite partial melt: experimental constraints on the mantle source of Hawaiian basalts. *Contributions to Mineralogy and Petrology* **156**, 661–678.

Wolfe, C. J., Solomon, S. C., Laske, G., Collins, J. A., Detrick, R. S., Orcutt, J. A., Bercovici, D. & Hauri, E. H. (2009). Mantle shear-wave velocity structure beneath the Hawaiian hot spot. *Science* **326**, 1388–1390.

Yasuda, A., Fujii, T. & Kurita, K. (1994). Melting phase relatins of an anhydrous mid-ocean ridge basalt from 3 to 20 GPa: Implications for the behavior of subducted oceanic crust in the mantle. *Journal of Geophysical Research* **99**, 9401–9414.

Yaxley, G. M. & Sobolev, A. V. (2007). High-pressure partial melting of gabbro and its role in the Hawaiian magma source. *Contributions to Mineralogy and Petrology* **154**, 371–383.